

NUCLEAR DATA AND MEASUREMENTS SERIES

ANL/NDM-138

Neutron Scattering and Models: Chromium

by

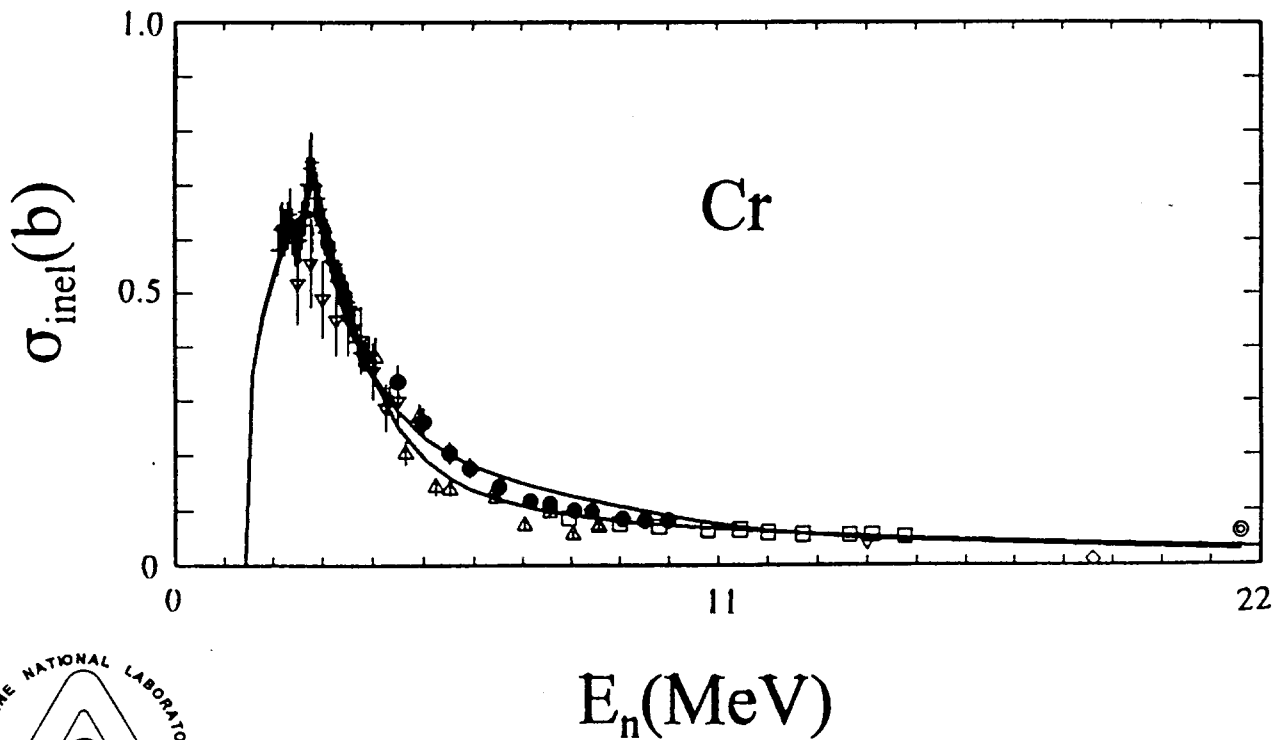
A.B. Smith and D. Schmidt

June 1996

**ARGONNE NATIONAL LABORATORY,
ARGONNE, ILLINOIS 60439, U.S.A.**

NUCLEAR DATA AND MEASUREMENTS SERIES

ANL/NDM-138
NEUTRON SCATTERING AND MODELS:-CHROMIUM
A. B. Smith and D. Schmidt
June, 1996



ARGONNE NATIONAL LABORATORY, ARGONNE, ILLINOIS
Operated by THE UNIVERSITY OF CHICAGO
for the U. S. DEPARTMENT OF ENERGY
under Contract W-31-109-Eng-38

Argonne National Laboratory

Argonne National Laboratory, with facilities in the states of Illinois and Idaho, is owned by the United States Government, and operated by the University of Chicago under provisions of a contract with the Department of Energy.

Disclaimer

This report was prepared as an account of work sponsored by an agency of the United States Government. Neither the United States Government nor any agency thereof, nor any of their employees, makes any warranty, express or implied, or assumes any legal liability or responsibility for the accuracy, completeness, or usefulness of any information, apparatus, product, or process disclosed, or represents that its use would not infringe privately owned rights. Reference herein to any specific commercial product, process, or service by trade name, trademark, manufacturer, or otherwise, does not necessarily constitute or imply its endorsement, recommendation, or favoring by the United States Government or any agency thereof. The views and opinions of authors expressed herein do not necessarily state or reflect those of the United States Government or any agency thereof.

Reproduced from the best available copy.

Available to DOE and DOE contractors from the Office of Scientific and Technical Information, P. O. Box 62, Oak Ridge, TN 37831; prices available from (423) 576-8401.

Available to the public from the National Technical Information Service, U. S. Department of Commerce, 5285 Port Royal Road, Springfield, VA 22161.

ANL/NDM-138

NEUTRON SCATTERING AND MODELS:- CHROMIUM*

by

A. B. Smith^{a,b} and D. Schmidt^c

^aArgonne National Laboratory Argonne, IL, USA

^bThe University of Arizona, Tucson, AZ, USA

^cPhysikalisch-Technische Bundesanstalt,
Braunschweig, Germany

June, 1996

Keywords:

Measured $d\sigma/d\Omega_{el}$ and $d\sigma/d\Omega_{inel}$ 4.5 → 10 MeV neutrons incident on elemental chromium. Comprehensive optical and coupled-channels model interpretations.

* This work supported by the United States Department of Energy under contract W-31-109-Eng-38, and by the Nuclear and Energy Engineering Program, College of Engineering and Mines, The University of Arizona.

PUBLICATIONS IN THE ANL/NDM SERIES

A listing of recent issues in this series is given below. Issues and/or titles prior to ANL/NDM-120 can be obtained from the National Technical Information Service, U. S. Department of Commerce, 5285 Port Royal Road, Springfield, VA 22161, or by contacting the author of this report at the following address:-

Technology Development Division
Argonne National Laboratory
9700 South Cass Avenue
Argonne, IL 60439
USA

- A. B. SMITH, P. T. GUENTHER, J. F. WHALEN, AND S. CHIBA
Fast-neutron Total and Scattering Cross Sections of ^{58}Ni and Nuclear Models
ANL/NDM-120, July 1991
- S. CHIBA AND D. L. SMITH
A Suggested Procedure for Resolving an Anomaly in Least-squares Data Analysis Known as "Peelle's Pertinent Puzzle" and the General Implications for Nuclear Data Evaluation
ANL/NDM-121, September 1991
- D. L. SMITH AND DOMINIQUE FEAUTRIER
Development and Testing of a Deuterium Gas Target Assembly for Neutron Production Via the $\text{H-2}(D,N)\text{HE-3}$ Reaction at a Low-energy Accelerator Facility
ANL/NDM-122, March 1992
- D. L. SMITH AND E. T. CHENG
A Review of Nuclear Data Needs and Their Status for Fusion Reactor Technology with some Suggestions on a Strategy to Satisfy the Requirements
ANL/NDM-123, September 1991
- J. W. MEADOWS
The Thick-Target $^9\text{Be}(d,n)$ Neutron Spectra for Deuteron Energies Between 2.5 and 7.0-MeV
ANL/NDM-124, November 1991
- A. B. SMITH AND P. T. GUENTHER
Fast-Neutron Scattering Near Shell Closures:- Scandium
ANL/NDM-125, August 1992
- A. B. SMITH, J. W. MEADOWS AND R. J. HOWERTON
A Basic Evaluated Neutronic Data File for Elemental Scandium
ANL/NDM-126, November 1992

- A. B. SMITH AND P. T. GUENTHER
Fast-Neutron Interaction With Vibrational Cadmium Nuclei
ANL/NDM-127, November 1992
- D. L. SMITH
A Least-Squares Computational "Tool Kit"
ANL/NDM-128, April 1993
- JOSEPH McCABE, A. B. SMITH AND J. W. MEADOWS
Evaluated Nuclear Data Files for the Naturally-Occurring Isotopes of Cadmium
ANL/NDM-129, June 1993
- A. B. SMITH AND P. T. GUENTHER
Fast-Neutron Interaction with the Fission Product ^{103}Rh
ANL/NDM-130, September 1993
- A. B. SMITH AND P. T. GUENTHER
Fast-Neutron Scattering from Vibrational Palladium Nuclei
ANL/NDM-131, October 1993
- A. B. SMITH
Neutron Interaction with Doubly-Magic ^{40}Ca
ANL/NDM-132, December 1993
- A. B. SMITH
Neutron Scattering at $Z = 50$:- Tin
ANL/NDM-133, September 1994
- A. B. SMITH, S. CHIBA AND J. W. MEADOWS
An Evaluated Neutronic File for Elemental Zirconium
ANL/NDM-134, September 1994
- A. B. SMITH
Neutron Scattering from Elemental Uranium and Thorium
ANL/NDM-135, February 1995
- A. B. SMITH
Neutron Scattering and Models:- Iron
ANL/NDM-136, August 1995
- A. B. Smith
Neutron Scattering and Models:- Silver
ANL/NDM-137, June 1996

TABLE OF CONTENTS

	page
Abstract -----	1
1. Introduction -----	2
2. Experimental Methods -----	2
3. Experimental Results -----	3
4. Interpretations -----	10
5. Discussion and Summary -----	18
Acknowledgments -----	35
References -----	37

NEUTRON SCATTERING AND MODELS:- CHROMIUM

by

A. B. Smith^{a,b} and D. Schmidt^c

^aArgonne National Laboratory

^bThe University of Arizona

^cPhysikalisch-Technische Bundesanstalt

Abstract

Differential neutron elastic-scattering cross sections of elemental chromium are measured from 4.5 → 10 MeV in steps of ≈ 0.5 MeV and at >≈ 40 scattering angles distributed between ≈ 17° → 160°. Concurrently differential cross sections for the inelastic neutron excitation of the yrast 2⁺ (1.434 MeV) level in ⁵²Cr are determined. In addition, broad inelastically-scattered neutron groups are observed corresponding to composite excitation of levels up to ≈ 5.5 MeV in the various chromium isotopes. These experimental results are combined with low-energy values previously reported from this laboratory, with recent ≈ 8 → 15 MeV data measured at the Physikalisch-Technische Bundesanstalt and with a 21.6 MeV result from the literature to form an extensive neutron-scattering data base which is interpreted in the context of spherical-optical and coupled-channels (rotational and vibrational) models. These models reasonably describe the observables but indicate rather large energy-dependent parameter trends at low energies similar to those previously reported near the peak of the S₀ strength function in studies at this laboratory. The physical implications of the measurements and models are discussed including deformation, coupling, dispersive and asymmetry effects.

1. Introduction

Chromium finds wide use in fusion and fission energy systems as a major constituent of various stainless-steel alloys. As a consequence the respective neutron cross sections are of applied importance and some have been extensively studied. However, fast-neutron scattering above several MeV has not received particularly attention, and the available experimental results are fragmentary and often quite old [KP74, GSW82, Hom+69, Ols+87, Ste+65, CL56]. Elemental chromium consists of the four isotopes ^{50}Cr (4.345%), ^{52}Cr (83.790%), ^{53}Cr (9.500%) and ^{54}Cr (2.365%). The prominent ^{52}Cr isotope is magic in neutron number ($N = 28$) and is well represented by a proton core with four $h_{7/2}$ holes in the

closed shell [Joh+85, MBZ64]. The spectroscopy of ^{52}Cr has been extensively studied theoretically primarily using shell-model concepts, and experimentally using a wide variety of nucleon-transfer and knock-out reactions. The low-lying structure displays characteristics of a collective vibrator. Coulomb-excitation studies indicate large collective effects (e.g., $\beta_2 = 0.224$, [Ram+87]) and thus there should be relatively strong neutron-scattering direct reactions. These should be primarily with the proton core and consistent with the predictions of the core-coupling model [MBA75]. Studies of fast-neutron scattering in this mass region indicate very large absorption-potential strengths at low energies and substantial dispersion effects [Smi95]. The details are difficult to determine due to large fluctuations in the experimental data resulting from partially resolved and overlapping resonances even at rather high incident energies.

The present work was undertaken to provide basic data for applications and to give improved definition to the fundamental aspects of the neutron interaction with chromium. After completion of the present measurements, some very good scattering results became available from the Physikalisch-Technische Bundesanstalt (PTB) extending from $\approx 8 \rightarrow 15$ MeV [SM96]. These, combined with the present experimental values, result in a great improvement in the knowledge of neutron scattering from chromium, and make possible improved physical interpretations. The experimental method is briefly outlined in Section 2 and the experimental results presented in Section 3. Spherical-optical and coupled-channels model interpretations are described in Section 4, and physical implications are discussed and summary comments given in Section 5.

2. Experimental Methods

The Argonne measurements were made using the fast-neutron time-of-flight method [CL55] and the Argonne ten-angle detection system. This method and apparatus have been amply described

elsewhere [Smi+92] thus only details relevant to the present measurements are outlined here. The measurement sample was a cylinder of compressed sintered elemental chromium 2 cm in diameter and 2 cm long. It had a density approaching that of chromium metal and it was assumed that the chemical purity was 100%. However, in some of the measurements there was an indication that several atom-percent of oxygen was present. Such a contamination could not be verified and it is at most small so it was ignored. The $D(d,n)$ reaction was used as a neutron source with the deuterium contained in a 2 cm long gas cell [Dro87]. The pressure in the cell was such that the incident-neutron energy spreads decreased from ≈ 300 keV at 4 MeV to 100 keV at 10 MeV. The mean neutron energy was known to ≈ 10 keV. The neutron source was pulsed at a repetition rate of 2 MHz with a burst duration of ≈ 1 nsec. Ten neutron flight paths were distributed about the scattering sample with lengths of ≈ 500 cm, and the scattered neutrons were detected with hydrogenous scintillators. Scattered-neutron resolutions were sufficient to separate the elastically-scattered neutrons from those inelastically scattered from all the even isotopes of chromium ($\approx 91\%$ abundant). All of the cross sections were determined relative to the well-known $H(n,n)$ scattering standard [CSL83], and corrected for beam-attenuation, multiple-event and angular-resolution effects using Monte-Carlo techniques [Smi91]. The PTB measurements also employed the time-of-flight method. The measurement methodology and analysis procedure of the PTB data were similar to those described in ref. [Sch+94].

3. Experimental Results

3.1. Elastic neutron scattering

Differential elastic scattering measurements were made from 4.5 to 10 MeV in increments of ≈ 0.5 MeV, and at $\approx > 40$ scattering angles distributed between $\approx 17^\circ$ and 160° . The relative angular uncertainties are $< 0.1^\circ$ and the uncertainty in the absolute angular scale is $\approx 0.1^\circ$. The cross-section uncertainties are $\approx > 3\%$, with the largest values at the minima of the distributions, including consideration of statistical, normalization, correction and angular-resolution effects. These experimental results are summarized in Fig. 3.1. They well extrapolate to the lower-energy results previously reported from this laboratory [GSW82]. There are a few elastic-scattering values reported in the literature that are comparable with the present results [KP74, Hom+69]. They do not have the scope and/or detail of the present work, and the agreement with the present values varies, as illustrated in Fig. 3.2. The discrepancies may, in part, be due to the use of slightly different incident energies in a fluctuating environment. The three lowest energies of the very recent PTB elastic-scattering results [SM96] can be compared with the present measurements and

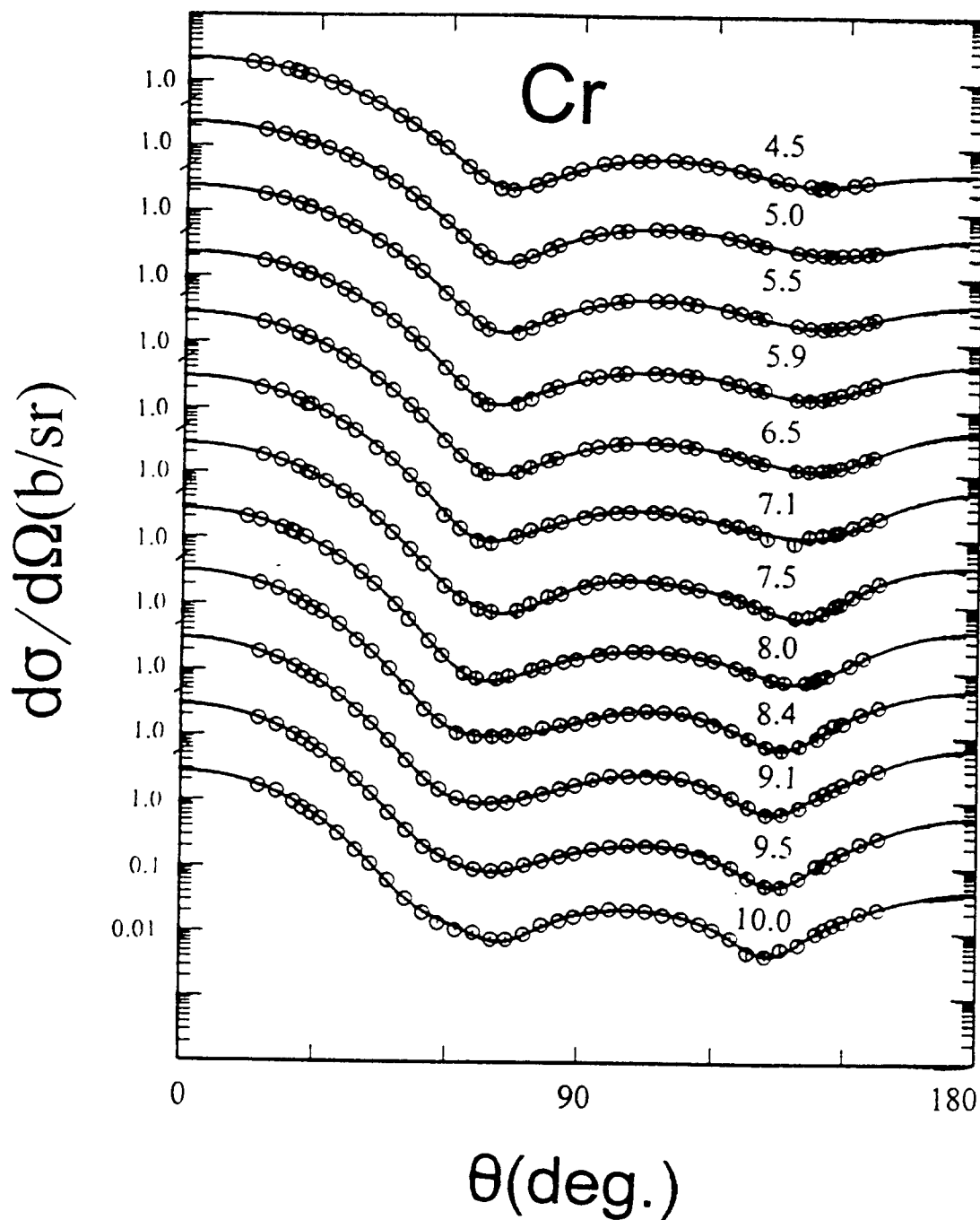


Fig. 3.1. Differential elastic-scattering cross sections of elemental chromium. The present work is indicated by symbols and curves show the results of fitting Legendre-polynomial series to the measured values. Approximate incident energies in MeV are numerically noted. Throughout this report differential distributions are given in the laboratory coordinate system.

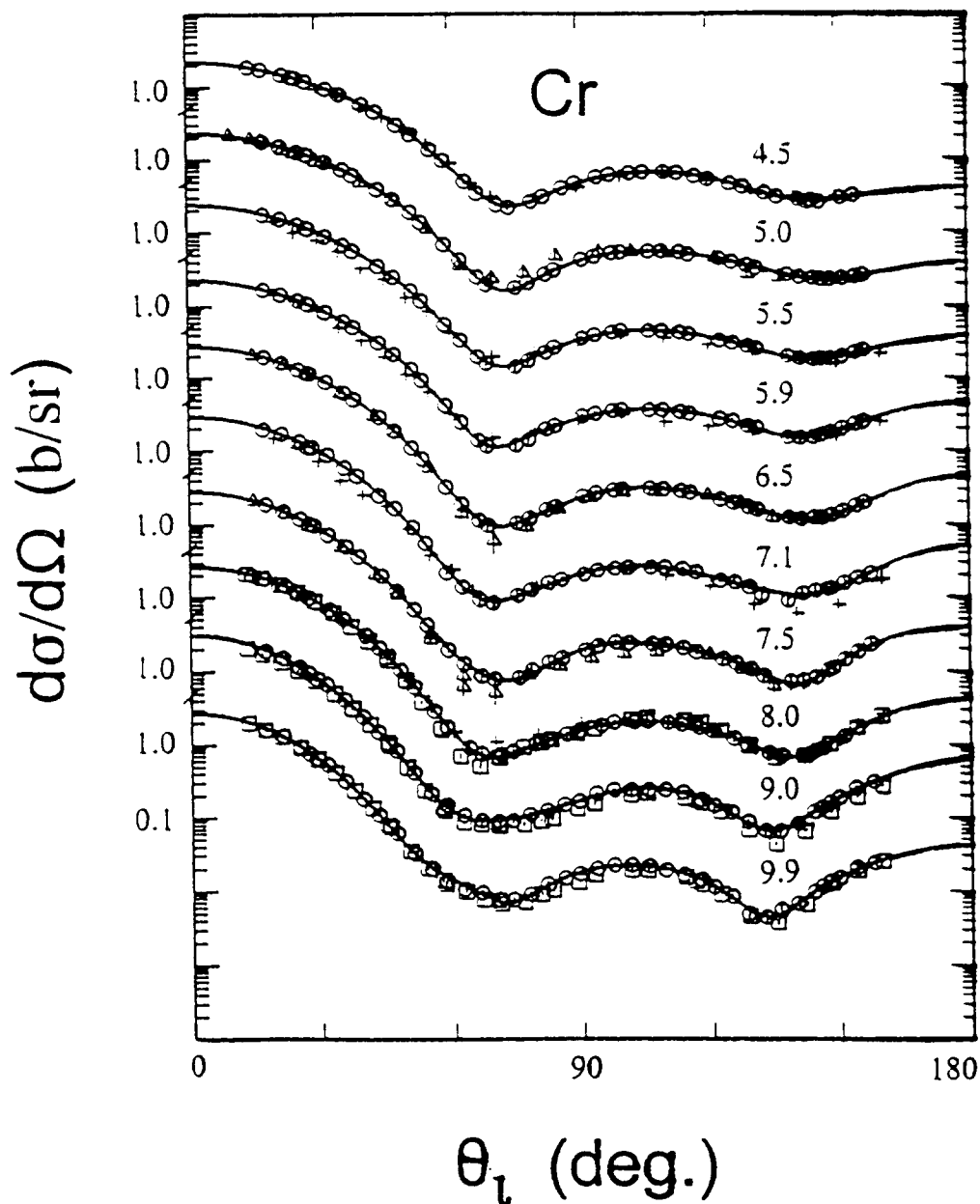


Fig. 3.2. Comparisons of the present elastic-scattering results (circular symbols) with values found in the literature (crosses from ref. [KP74], triangles from ref. [Hom+69]). Boxes indicate the recent PTB results [SM96]. Curves show Legendre-polynomial fits to the present results. Approximate incident energies are numerically noted in MeV.

the agreement is reasonably good (see Fig. 3.2).

3.2. Inelastic neutron scattering

Differential inelastic-scattering measurements were made concurrently with the elastic-scattering studies. Primary attention was focused on the excitation of the 1.434 MeV yrast 2^+ level of ^{52}Cr (herein level spins, parities and energies are taken from the Nuclear Data Sheets [NDS]). The measured differential cross sections for the excitation of the 1.434 MeV level are shown in Fig. 3.3. The indicated uncertainties are subjective estimates, including consideration of statistical, normalization and correction contributions. In several of the measurements some weak lower-energy excitations were observed. They were attributed to the minor isotopes of chromium and were ignored. There was also a trace of a neutron group that could be due to oxygen contamination of the sample, but the evidence was weak and thus that too was ignored. Angle-integrated inelastic-scattering cross sections were determined by fitting the measured differential distributions with Legendre-polynomial series, with the results for the excitation of the 1.434 MeV level shown in Fig. 3.4. Inelastic scattering due to excitations of $>\approx 2.5$ MeV consisted of contributions from clumps of levels which blended into a fluctuating continuum. These clumps were centered about excitations of approximately 3.0, 3.5, 3.9, 4.6, 5.4 and 5.8 MeV, and must be due to cumulative contributions from levels in the various chromium isotopes. The corresponding scattered neutrons were approximately isotropically distributed, with some tendency for the distributions to peak toward forward angles. Due to their probable complexity, no attempt was made to resolve the individual components. There are remarkably few experimental chromium inelastic-scattering cross sections reported in the literature. A number of $(n;n',\gamma)$ results have been reported but they do not directly provide inelastic-scattering cross sections. The present results reasonably extrapolate to the lower-energy values previously reported from this laboratory [GSW82] and to those reported in ref. [Ram75] (see Fig. 3.4). Some of the elemental and isotopic angle-integrated chromium results reported by Kinney and Perey [KP74] compare reasonably well with those of the present work as illustrated in Fig. 3.4. Where there are significant discrepancies they are generally associated with measurements of ref. [KP74] using only a very few scattering angles. Where the work of ref. [KP74] employed a number of scattering angles the differential results are similar to those of the present work, as illustrated in Fig. 3.5. In addition, there are three comparable inelastic-scattering differential distributions from the recent PTB measurements [SM96]. These are in quite good agreement with the present results, as shown in Fig. 3.5, excepting the very forward angles where the results of ref. [SM96] tend to be lower.

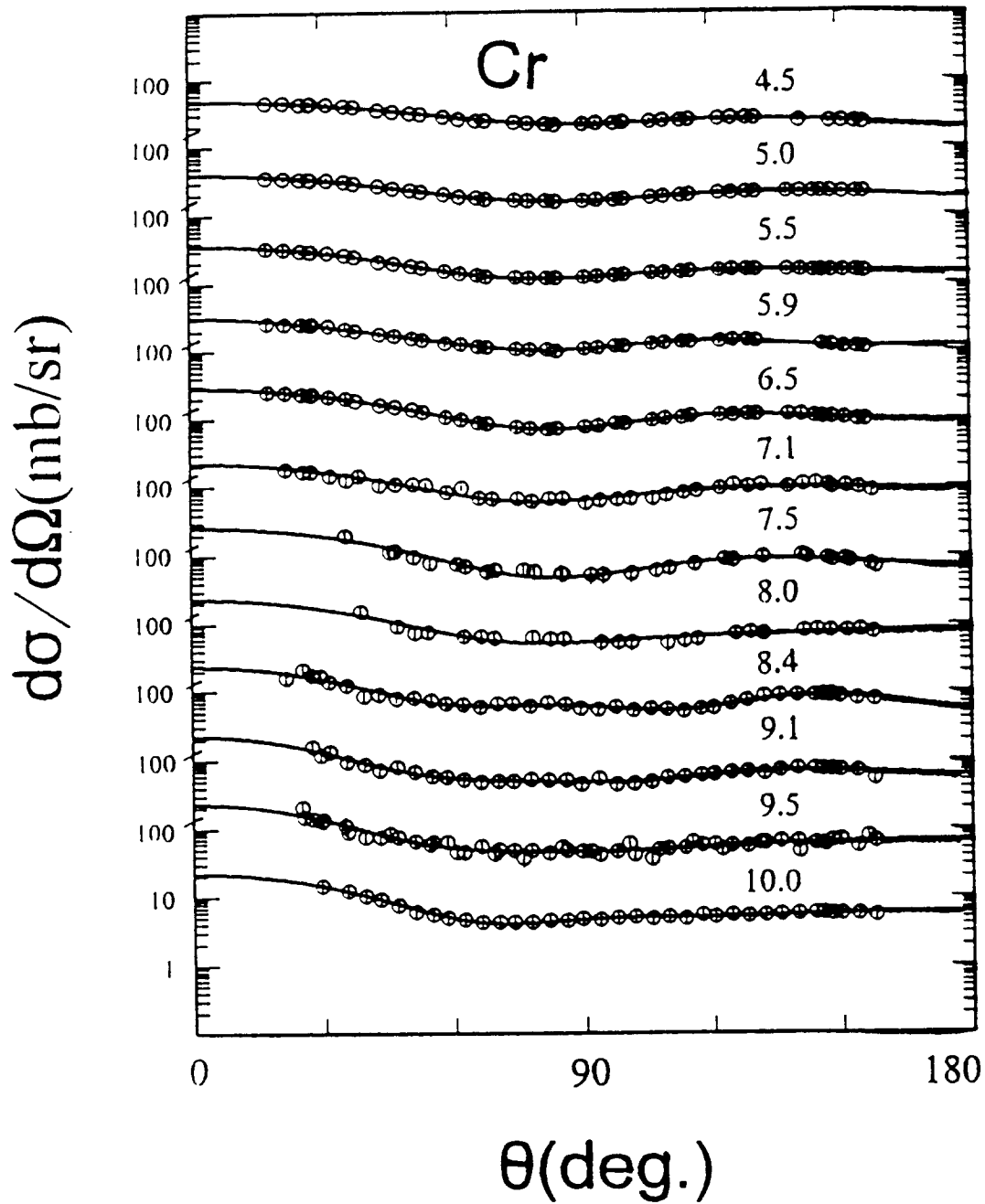


Fig. 3.3. Elemental differential neutron cross sections for the excitation of the 1.434 MeV level in ^{52}Cr . The present measured values are indicated by symbols and curves show the results of fitting Legendre-polynomial series to the experimental values. Approximate incident-neutron energies are numerically noted in MeV.

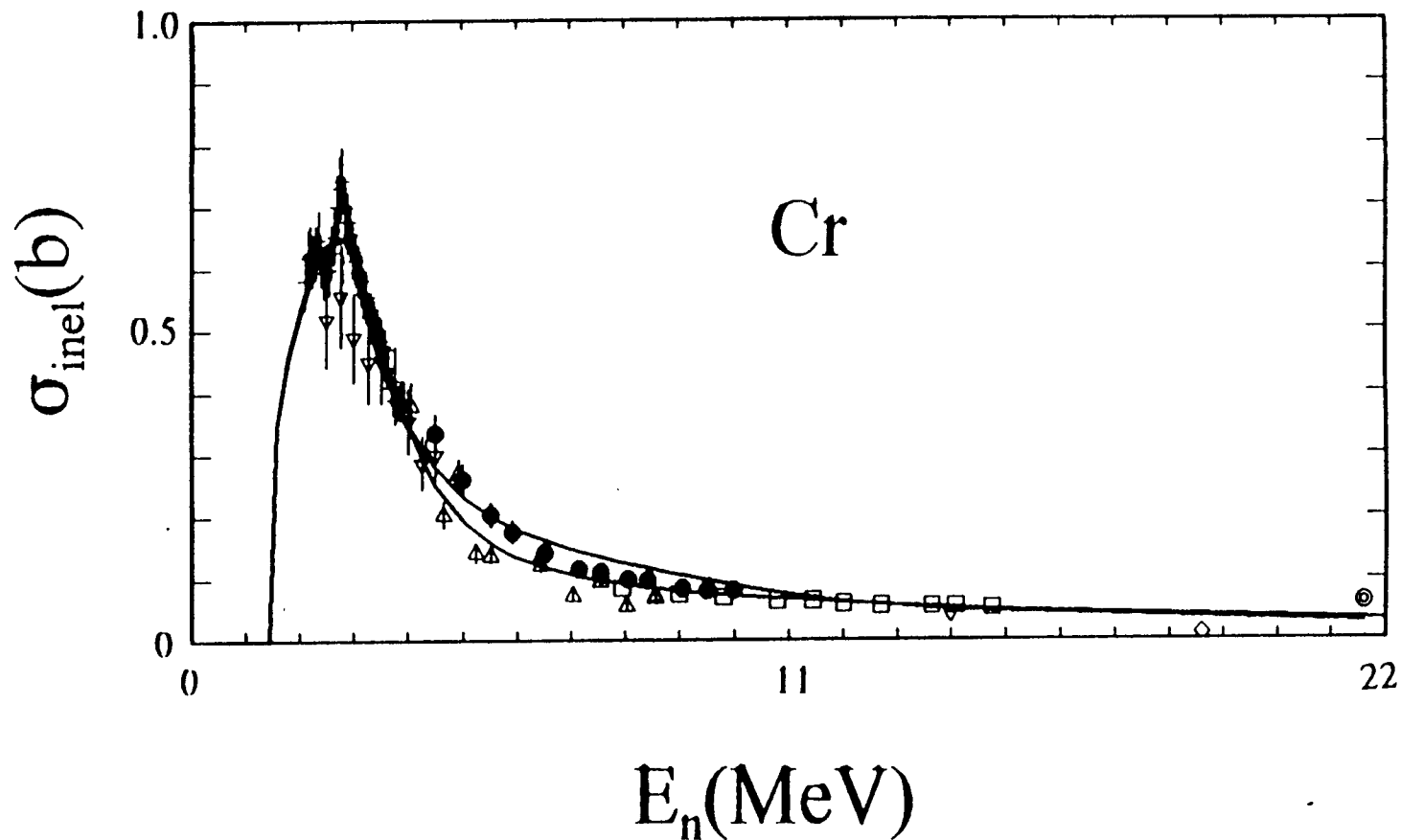


Fig. 3.4. Angle-integrated elemental cross sections for the excitation of the 1.434 MeV level of ^{52}Cr . The present results are indicated by solid circular symbols, those from earlier work from this laboratory by crosses, and the recent PTB values [SM96] by boxes. Other symbols indicate values taken from the literature [Ram75, KP74, CL56, TO67, Ste+65, Yam+90]. The curves indicate the results of model calculations as discussed in Section 4 of the text. The lower curve is based upon the statistical parameters of ref. [GC65]. The upper curve was obtained by increasing the temperature used in the calculations by 50%.

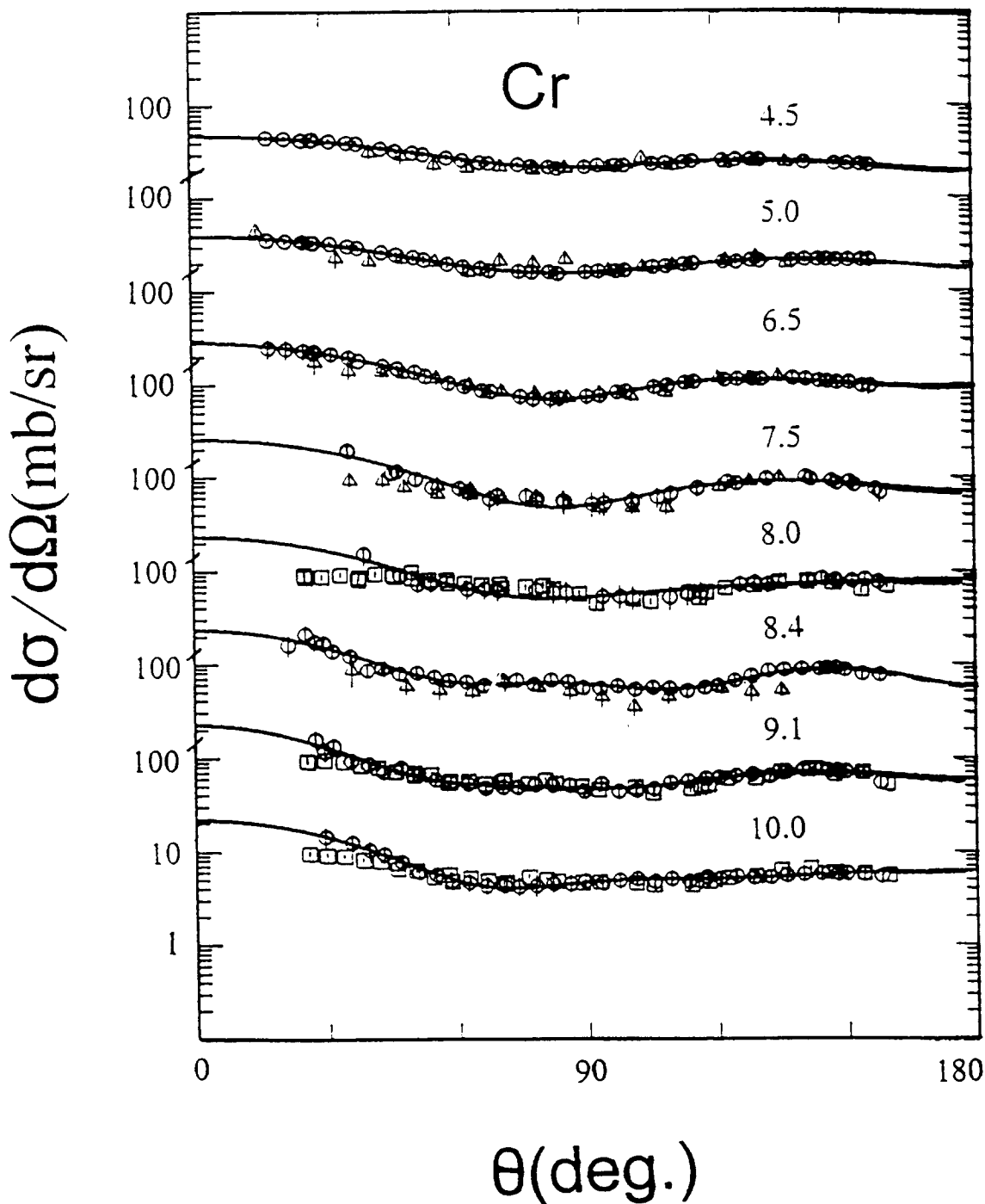


Fig. 3.5. Comparison of elemental differential cross sections for the excitation of 1.434 MeV level in ^{52}Cr . The present results are indicated by circular symbols and those of ref. [KP74] by triangles. The recent PTB values [SM96] are noted by boxes. Curves indicate the results of fitting Legendre-polynomial series to the present results. Approximate incident energies are numerically cited in MeV.

4. Interpretations

The above experimental results were interpreted in the context of a spherical optical model (SOM) and of a vibrational coupled-channels model (CCM). The SOM is clearly inappropriate for a strong collective nucleus, such as ^{52}Cr , but it is a useful vehicle in some applied and basic contexts (e.g., as a basis for DWBA calculations). Both of the interpretations were based primarily on χ^2 fitting of elastic-scattering data. The data base used in the fitting was constructed from:- i) the 1.5 \rightarrow 4 MeV results of ref. [GSW82], averaged over 200 keV to smooth fluctuations, ii) the present results from 4.5 \rightarrow 10 MeV, iii) the very recent \approx 8 \rightarrow 15 MeV data from PTB [SM96], and iv) the 21.6 MeV elastic distribution of ref. [Ols+87]. The complete elastic-scattering data base is shown in Fig. 4.1. There are a number of elastic-scattering results at energies of $<$ 1.5 MeV. They were not used in the interpretations as the data strongly fluctuate due to partially resolved resonance structure, and doorway effects may be present. Such behavior is not consistent with the concept of a SOM or CCM. There are a few additional elemental or isotopic elastic distributions above 1.5 MeV [NNDC]. They were not used as they were either inconsistent with the body of the information or were of limited angular scope and/or definition that compromised the fitting. In addition, subjective consideration was given to total cross sections using energy averages of the experimental results of refs. [MW66], [Cie+68] and [LHH81]; to inelastic scattering using the present results, those from the recent PTB measurements [SM96], earlier lower-energy results from this laboratory [GSW82] and scattered values from the literature [NNDC]; and to low-energy strength functions as given in the compilation of ref. [MDH81].

The χ^2 fitting employed the five-step procedure long used at this laboratory and extensively described previously [Smi+92]. It follows a convergent path first fixing the real-potential diffuseness a_v , then the real-potential radius r_v , then the imaginary-potential radius r_w , followed by the imaginary-potential diffuseness a_w , and finally the real and imaginary potential strengths J_v and J_w , respectively. Herein, unless otherwise stated, potential strengths are expressed as volume-integrals-per-nucleon and radii in the reduced form r_i , where the full radius $R_i = r_i \cdot A^{1/3}$. All of the SOM calculations employed versions of the computer code ABAREX [Mol81]. The CCM calculations used the codes ANLECIS, ECIS94 and ECIS95. All of these coupled-channels codes are based upon the work of J. Raynal [Ray94, Mol82]. The most recent version, ECIS95, offers a unique capability for treating problems of the present nature. Compound-nucleus (CN) effects were calculated up to 15 MeV using the Hauser-Feshbach method [HF52], with the resonance width

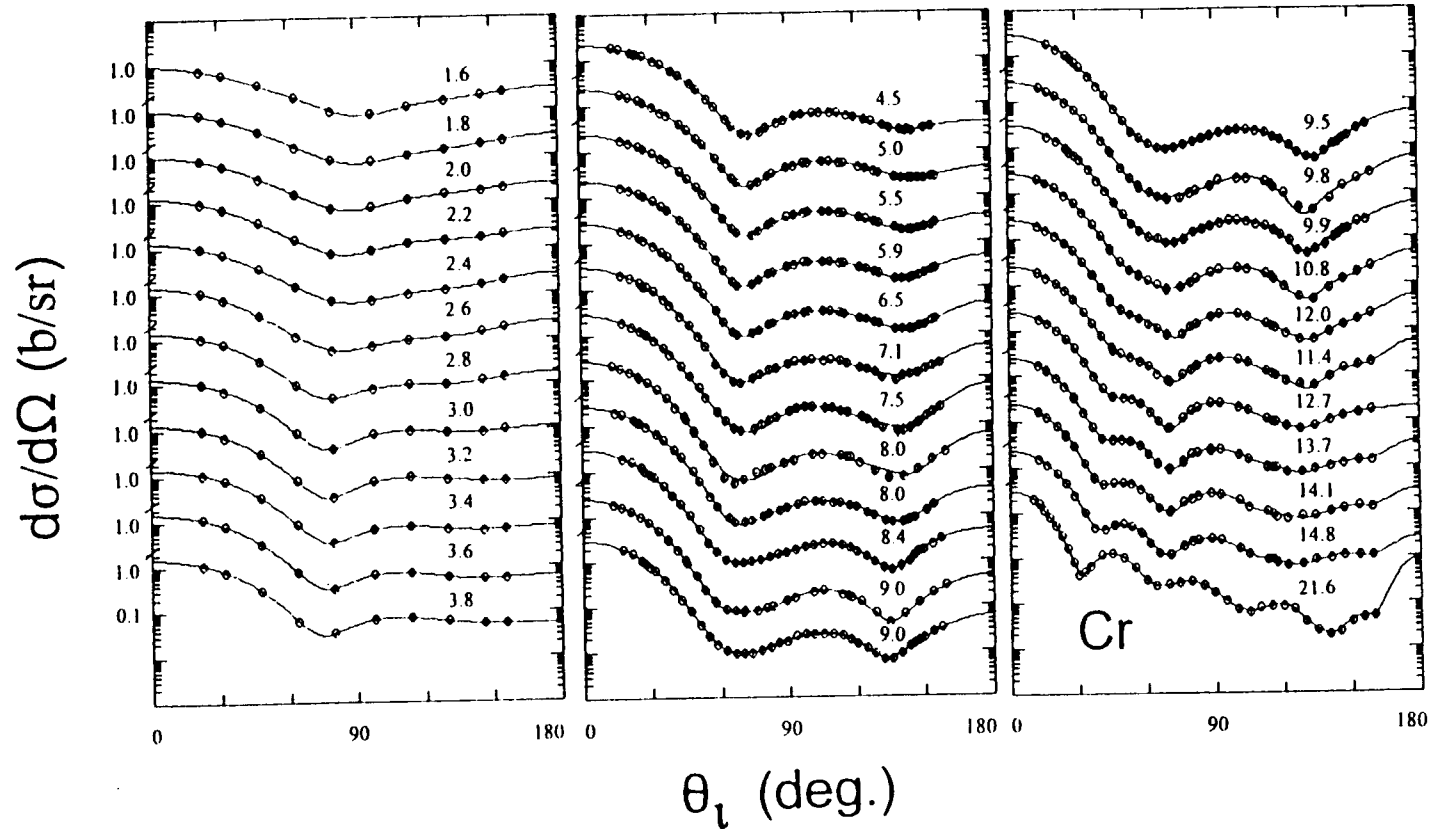


Fig. 4.1. Elastic-scattering data base used in the model interpretations. The measured values are indicated by circular symbols and curves show the results of fitting Legendre-polynomial expansions to the measured values. Approximate incident energies are numerically noted in MeV.

fluctuation and correlation corrections [Mol80]. At 21.6 MeV the elastic scattering was assumed to be entirely shape scattering. The necessary discrete level properties were taken from the Nuclear Data Sheets [NDS]. Higher-energy excitations were treated statistically using the method and parameters of Gilbert and Cameron [GC65]. All of the illustrated calculated results to incident energies of 15 MeV include the CN contribution. Charged-particle emission channels were ignored as their contribution is small at the energies where CN contributions are important to the interpretation. The real potential was assumed to have the Saxon-Woods (SW) form, the imaginary potential the SW-derivative form and the spin-orbit potential the Thomas form [Hod71]. The spin-orbit potential was assumed non-deformed and real, with the parameters taken from ref. [WG86]. Where relevant, the volume-absorption potential was taken to have the SW form and the geometries of the real potential.

4.1. The SOM model

Two versions of the SOM were derived. In one the elastic-scattering data base was concurrently fitted considering contributions from the four isotopes ^{50}Cr , ^{52}Cr , ^{53}Cr and ^{54}Cr . The calculations dealt explicitly with the discrete levels of each isotope up to excitations of ≈ 3.8 MeV for ^{50}Cr (12 levels), up to ≈ 4 MeV for ^{52}Cr (14 levels), up to ≈ 2.7 MeV for ^{53}Cr (12 levels, combining g.s. and first-excited-state contributions to be consistent with the experimental resolution), and up to ≈ 3.3 MeV for ^{54}Cr (8 levels). This model was termed the "elemental" model, or "ESOM". The resulting parameters of this ESOM are given in Table 4.1. The elastic-scattering calculated with the ESOM is compared with the measured values in Fig. 4.2, and Fig. 4.3 compares ESOM calculated and measured neutron total cross sections. Of course, the ESOM can not describe the prominent inelastic scattering as it makes no provision for the considerable direct-reaction component. The derivation of the ESOM involves extensive calculations including all four isotopes. Such calculations are not very practical for coupled-channels interpretations and thus one assumes that the element consists entirely of the prominent isotope ^{52}Cr ($\approx 84\%$ abundant). For comparison and reference purposes, that assumption was also made in the derivation of a spherical "isotopic" model, or "ISOM", based entirely on the isotope ^{52}Cr , following the same procedures used for obtaining the ESOM. The resulting parameters are given in Table 4.2, and a comparison with the data base is shown in Fig. 4.4. Total cross sections calculated with the ISOM are indistinguishable from those obtained with the ESOM potential.

Table 4.1*. Potential parameters of the ESOM model of the text. Strengths are given as volume-integrals-per-nucleon (in units of MeV-fm³), except for the spin-orbit potential where it is given in MeV. Energies, E, are in MeV and dimensions in fermis.

Real Potential

$$\begin{aligned}J_v &= 483.3 - 4.3501 \cdot E \\r_v &= 1.2914 - 0.002578 \cdot E \\a_v &= 0.6027\end{aligned}$$

Imaginary Potential

$$\begin{aligned}J_w &= 145.0 - 11.480 \cdot E \quad (E < 6.0) \\&= 73.4 + 0.46027 \cdot E \quad (E \geq 6.0) \\r_w &= 1.4139 - 0.033937 \cdot E + 0.00095713 \cdot E^2 \\a_w &= 0.100 + 0.076666 \cdot E \quad (E < 6) \\&= 0.5338 + 0.004375 \cdot E \quad (E \geq 6)\end{aligned}$$

Spin-orbit Potential

$$\begin{aligned}V_{so} &= 5.921 - 0.015 \cdot E \\r_{so} &= 1.103 \\a_{so} &= 0.560\end{aligned}$$

* Throughout this work potential parameters are given to precisions that make possible accurate reproduction of the calculated values. This precision does not necessarily imply uncertainty. The latter is more realistically three to four significant figures.

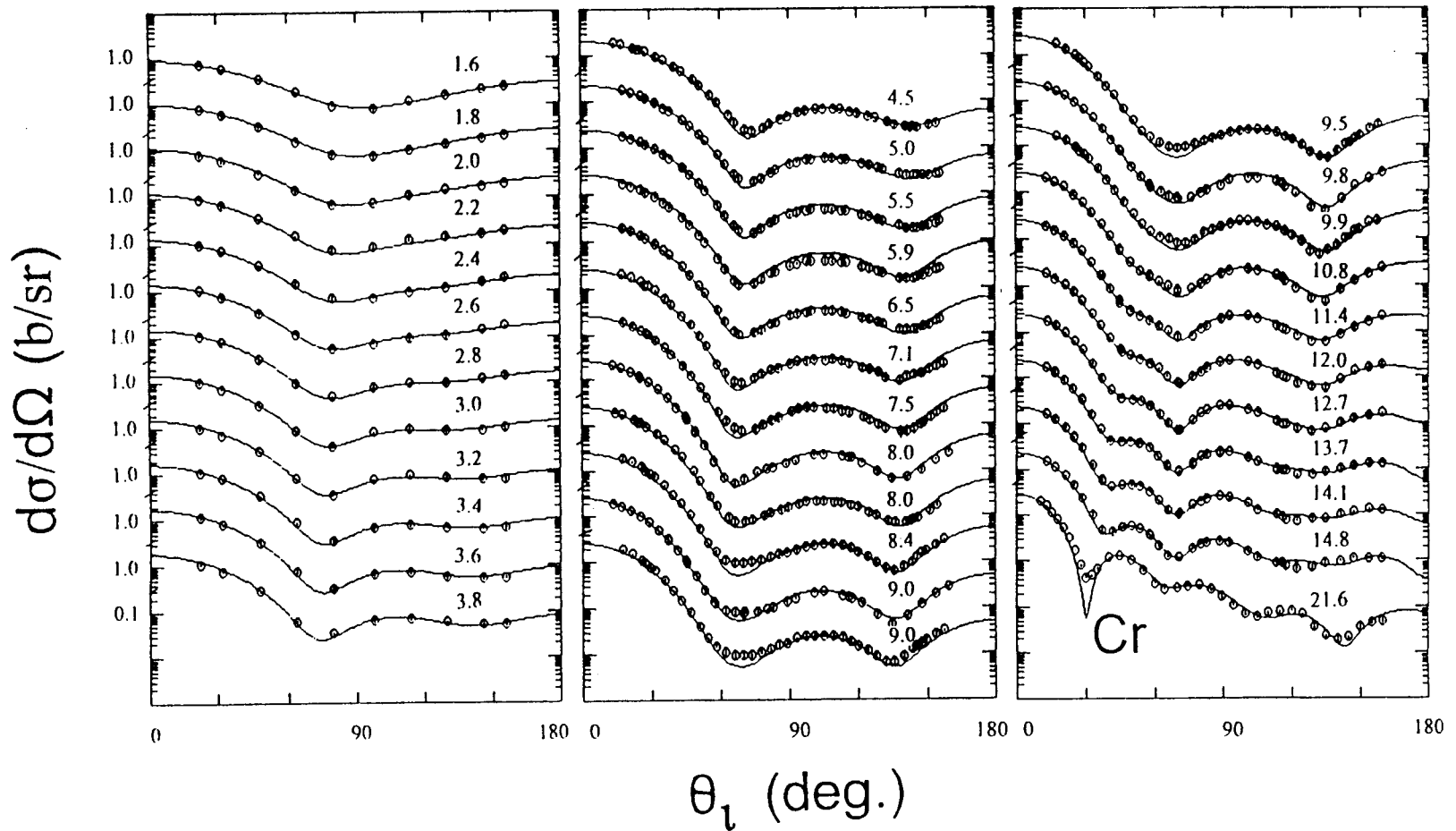


Fig. 4.2. Comparison of the measured elastic-scattering data base (symbols) with the results of ESOM calculations (curves). Approximate incident-neutron energies are numerically noted in MeV.

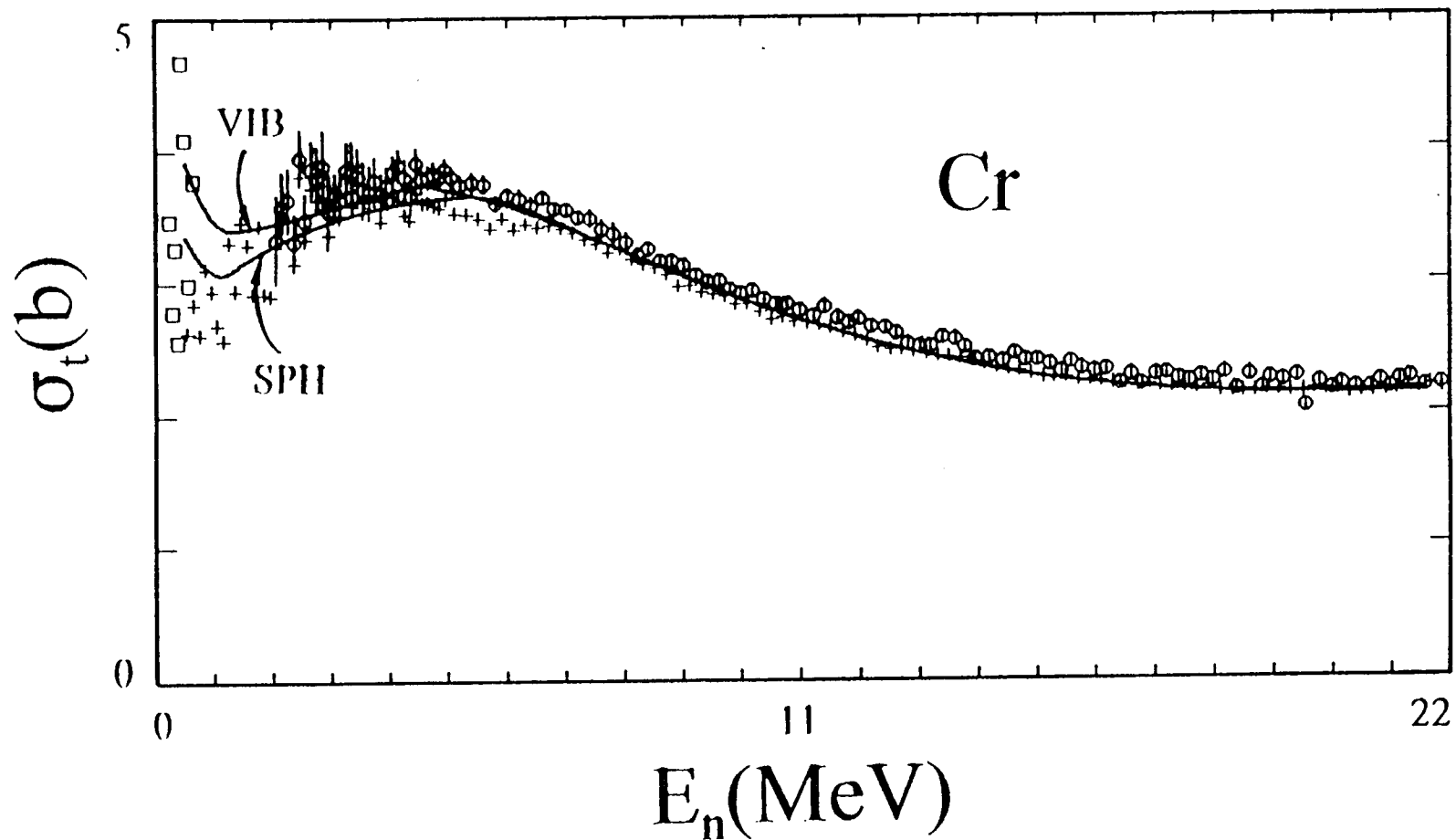


Fig. 4.3. Comparison of energy averages of measured neutron total cross sections (symbols; \square = ref. [MW66], \circ = ref. [LHH81], $+$ = ref. [Cie+68]) with the results of model calculations (curves). "VIB" denotes the vibrational CCM and "SPH" the ESOM of the text.

Table 4.2. Potential parameters of the ISOM of the text. The nomenclature is identical to that of Fig. 4.1.

Real Potential

$$\begin{aligned}J_v &= 492.2 - 5.7767 \cdot E \\r_v &= 1.3308 - 0.0071913 \cdot E \\a_v &= 0.5088 + 0.0075653 \cdot E\end{aligned}$$

Imaginary Potential

$$\begin{aligned}J_w &= 157.0 - 15.26 \cdot E \quad (E < 5.5) \\&= 68.5 + 0.81901 \cdot E \quad (E \geq 5.5) \\r_w &= 1.3032 - 0.015382 \cdot E \\a_w &= 0.10 + 0.09137 \cdot E \quad (E < 5.5) \\&= 0.5413 + 0.011124 \cdot E \quad (E \geq 5.5)\end{aligned}$$

Spin-orbit Potential

$$\begin{aligned}V_{so} &= 5.921 - 0.015 \cdot E \\r_{so} &= 1.103 \\a_{so} &= 0.560\end{aligned}$$

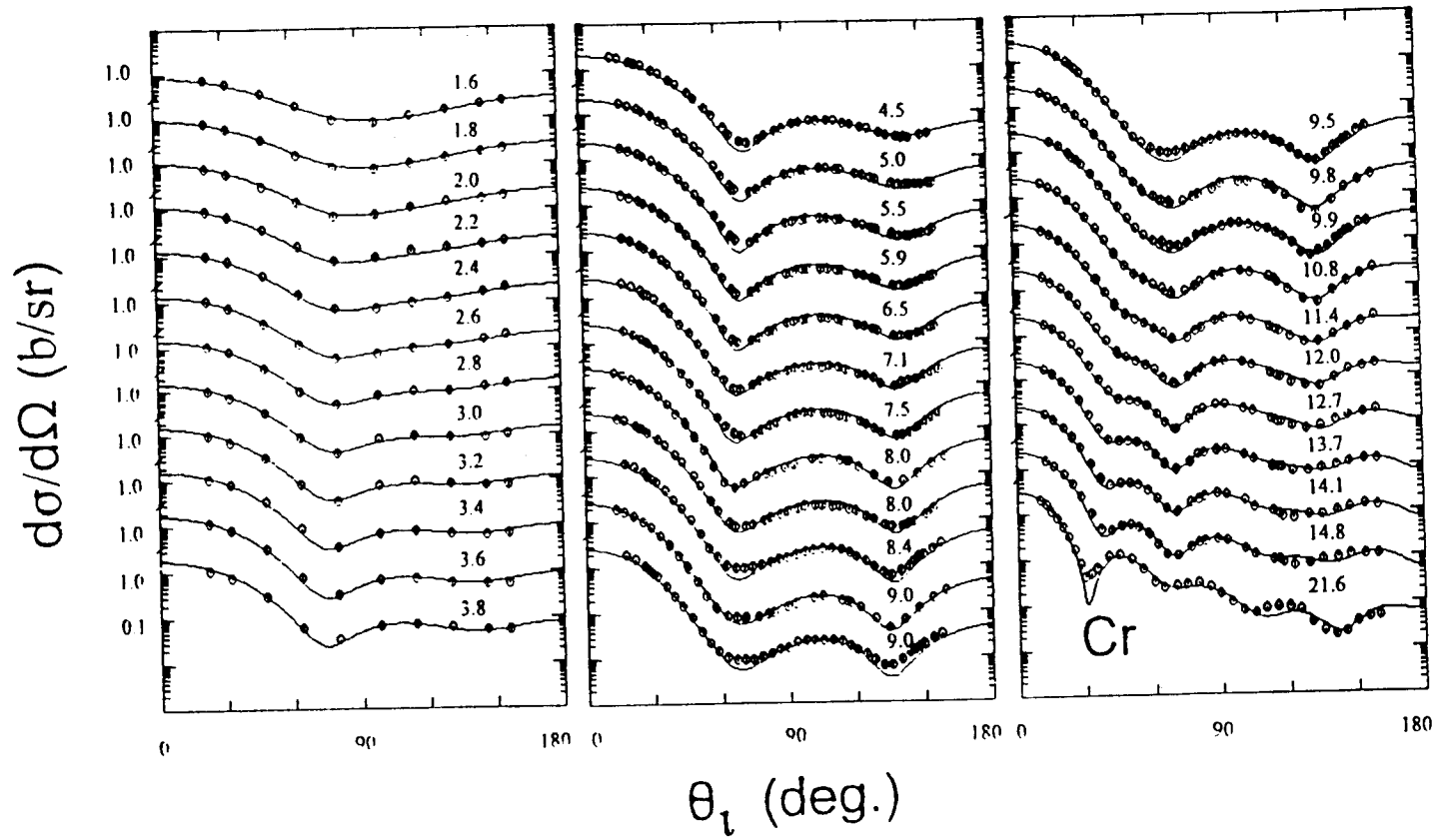


Fig. 4.4. Comparison of the measured elastic-scattering data base (symbols) with the results of ISOM calculations (curves). Approximate incident energies are numerically cited.

4.2. The CCM Model

Deducing the CCM model from the elemental data, including explicit treatment of the contributions of all isotopes, is formidable. Therefore, the target was assumed to be entirely ^{52}Cr . That is a reasonable assumption in view of the abundance of that isotope and the similar results obtained with the ESOM and ISOM, above. CN processes were treated as for the ISOM spherical model only, of course, using transmission coefficients calculated with the deformed potential. It was assumed that ^{52}Cr could be represented as a simple one-phonon vibrator. Coulomb-excitation considerations suggest a $\beta_2 = 0.224$ [Ram+87].

However, the entire χ^2 fitting procedure was repeated for β_2 values extending from 0.100 to 0.275 in steps of 0.025. All the resulting potentials reasonably described the elastic-scattering data base from which they were derived with no clear choice of deformation. However, the energy dependencies of the parameters obtained for large deformations (e.g., for $\beta_2 \approx 0.25 \rightarrow 0.275$) were "odd" and thus those results were abandoned. There is reasonable experimental knowledge of the cross sections for the excitation of the 1.434 MeV 2+ level up to ≈ 15 MeV. Thus experimental values from ≈ 8 to 15 MeV were used to determine the β_2 in the fitting. Lower-energy calculated results may be biased by uncertainties in the CN contribution, and at higher energies the experimental result of the literature appear discrepant. The result is $\beta_2 = 0.20 \pm \approx 0.01$. Larger or smaller values of β_2 led to experimentally unacceptable calculated inelastic-scattering results. With $\beta_2 = 0.200$ the CCM potential parameters of Table 4.3 were obtained. The calculated elastic-scattering results are compared with experimental values in Fig. 4.5. Calculated cross sections for the excitation of the 1.434 MeV level are compared with the measured angle-integrated values in Fig. 3.4 (the two curves in the figure are discussed in Section 5) and with the corresponding differential values in Fig. 4.6 (all illustrated inelastic-scattering cross sections include the CN contribution). Fig. 4.3 compares the experimental total neutron cross sections with those calculated with the CCM.

5. Discussion and Summary

The ESOM, ISOM and CCM give very similar elastic-scattering results all of which are quite descriptive of the experimental data from which the models were derived, as illustrated in Figs. 4.2, 4.4 and 4.5. The calculated results in the first minima of the distributions are somewhat lower than the measured values in the $\approx 9 \rightarrow 10$ MeV region, particularly for the spherical potentials. This may be partly an experimental problem as multiple-scattering corrections to the measured quantities are

Table 4.3. Potential parameters of the CCM of the text. The nomenclature is identical to that of Table 4.1.

Real Potential

$$\begin{aligned}J_v &= 495.7 - 5.0428 \cdot E \\r_v &= 1.2911 - 0.0023653 \cdot E \\a_v &= 0.6199\end{aligned}$$

Imaginary Potential

$$\begin{aligned}J_w &= 130.0 - 14.5 \cdot E \quad (E < 5.0) \\&= 51.0 + 1.3159 \cdot E \quad (E \geq 5.0) \\r_w &= 1.3526 - 0.015547 \cdot E \\a_w &= 0.2538 + 0.040266 \cdot E - 0.00090726 \cdot E^2\end{aligned}$$

Spin-orbit Potential

$$\begin{aligned}V_{so} &= 5.921 - 0.015 \cdot E \\r_{so} &= 1.103 \\a_{so} &= 0.560\end{aligned}$$

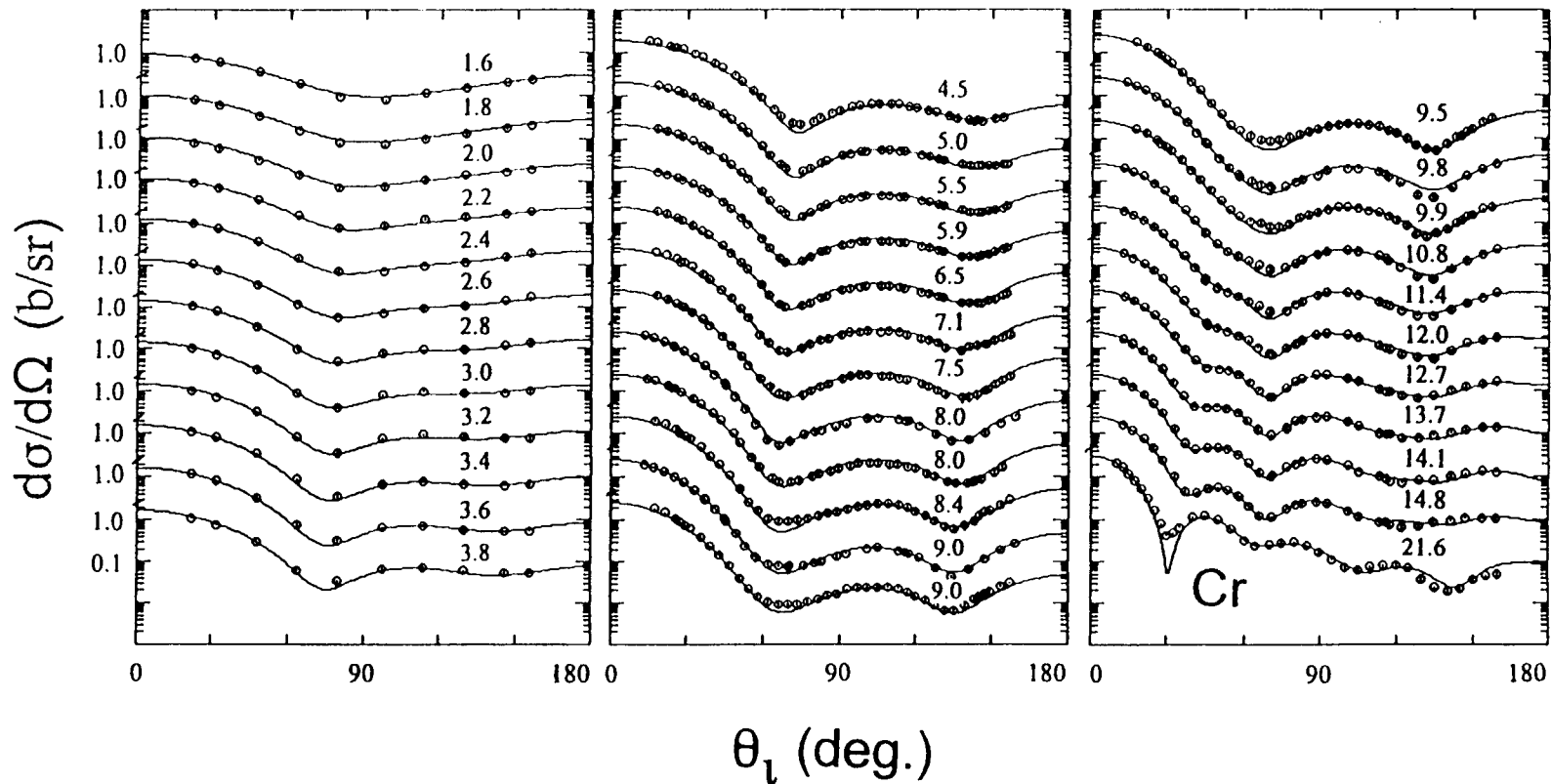


Fig. 4.5. Comparison of measured (symbols) and calculated (curves) differential elastic-scattering cross sections. The calculations were made with the CCM model of the text with $\beta_2 \approx 0.200$. Numerical values indicate approximate incident neutron energies in MeV.

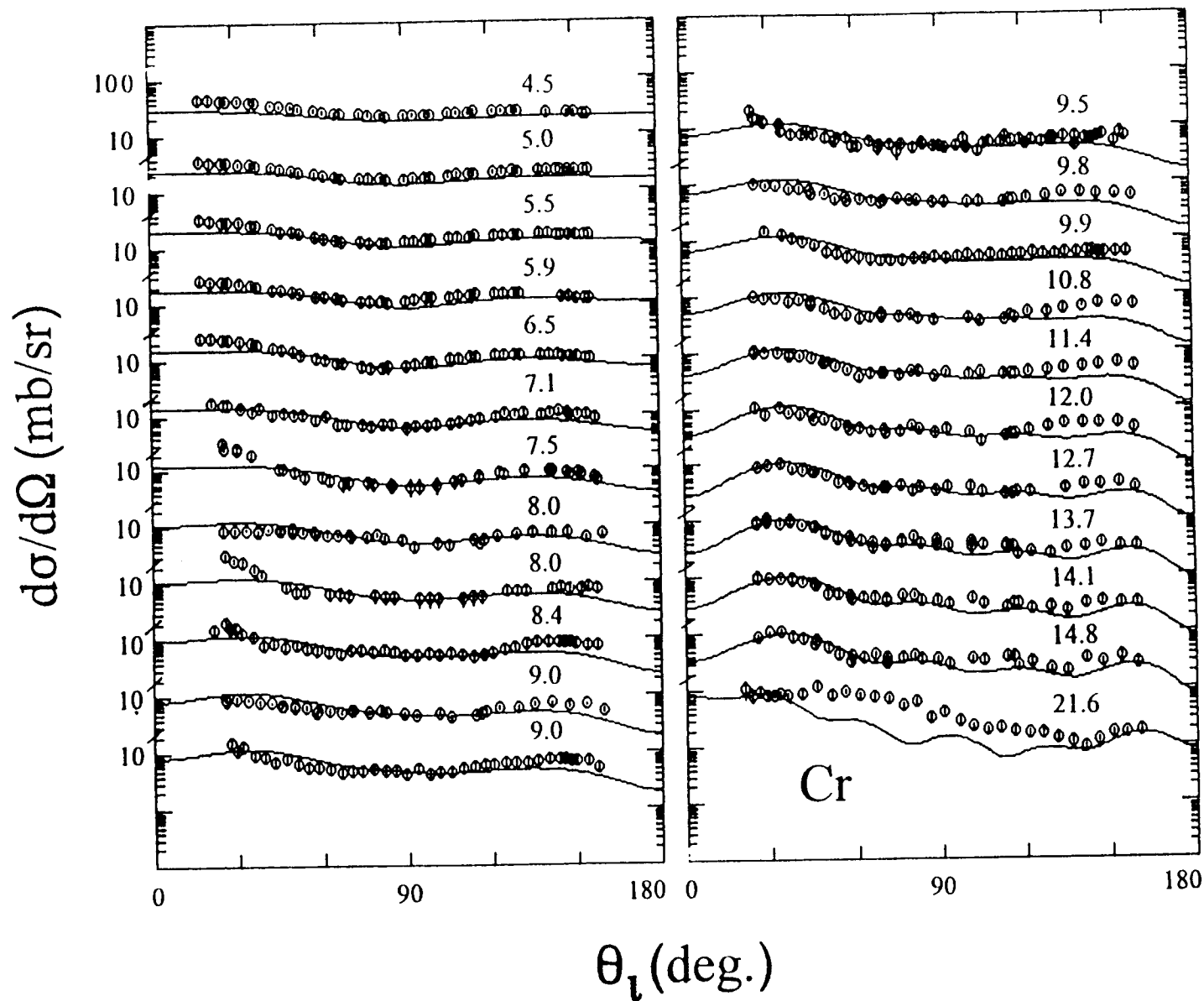


Fig. 4.6. Comparisons of measured (symbols) and calculated (curves) cross sections for the excitation of the 1.434 MeV level in ^{52}Cr using the CCM of the text with $\beta_2 = 0.200$. The values are presented on an elemental basis and numerical values indicate approximate incident energies in MeV.

very large in this region. On the other hand, independent data from two institutions agrees quite well, as illustrated in Fig. 3.2. There is a similar, only more acute, discrepancy between measured and calculated results at 21.6 MeV. That measured distribution is not entirely consistent with the model extrapolation of the lower-energy data, and the model fitting at higher energies is a compromise. Unfortunately, this is the only high-energy chromium elastic-scattering distribution and thus has a considerable weight in determining model energy dependencies, particularly in the present work as fluctuations compromise the fitting of low energy data. It is interesting that the authors of this particular set of data experienced considerable difficulties in describing this distribution with SOM and CCM models [Ols+87, Ols+90]. They too found calculated values at the first minimum of the elastic distribution far lower than the experimental data, and alleviated the problem by increasing the spin-orbit strength by $\approx 50\%$. That option is not attractive in the present case as the calculated descriptions at lower energies (e.g., ≈ 15 MeV) are compromised and there is no apparent physical justification supporting such large increases in spin-orbit strength. Generally, model interpretations of neutron scattering over a wide energy range tend to be compromised by the sparsity of accurate higher-energy neutron-scattering data; chromium is an acute example. It is clear that the elastic neutron scattering alone does not sharply differentiate between SOM and CCM models, much less the details of collective coupling schemes, as generally noted by Hodgson [Hod71].

Even rather broad energy averages of chromium neutron total cross sections fluctuate by large amounts at lower energies and there are significant differences between experimental results over wide energy ranges, as illustrated in Fig. 4.3. Given this situation, the total cross sections calculated with the ESOM (essentially the same values follow from the ISOM) and CCM reasonably describe the measured values (see Fig. 4.3). The two calculated results are very close to one another, to the experimental results of refs. [LHH81] and [Cie+68] from 2 \rightarrow 10 MeV, and closely follow the results of ref. [Cie+68] to higher energies. At the higher energies the agreement with the measured values is as good as the agreement between the two experimental data sets themselves. Both calculations give relatively small total cross sections in the 1 \rightarrow 1.5 MeV range, and tend toward the lower averages of the experimental values. This is in part the result of the energy dependencies of the model parameters. If the higher-energy branches of the models are used much larger total cross sections are obtained at ≈ 1 MeV. This dichotomy between models based upon high- and low-energy neutron data has long existed. The present models alleviate the situation through the use of energy-dependent parameters. It is noted that if one uses considerably larger spin-orbit strengths, as suggested in ref. [Ols+90], calculated total cross sections at higher energies fall two or more percent below the measured values. Models are not particularly sensitive to total neutron cross sections. This fact, together with the obvious low-energy fluctuations and the

few-percent discrepancy between measured chromium total cross sections, results in minimal guidance as to the choice between the present models.

It is common practice to test the low-energy behavior of models by comparing experimentally-derived and calculated strength functions. Such comparisons are given in Table 5.1. The measured and calculated S_0 values are in reasonable agreement. The ESOM and CCM results are consistent with the experimental value to within the experimental uncertainty alone, and the ISOM result is only slightly larger. The comparisons are not quite as favorable for the S_1 strength functions where the ESOM value is in very good agreement with the experimental result but the CCM result is somewhat larger. There are certainly large fluctuations in the low-energy resonance behavior of the chromium isotopes. Given this, the comparisons of measured and calculated strength functions is reasonably encouraging, and supports the large low-energy imaginary strengths of the present models. It is also clear that the comparisons give little guidance as to the choice of model.

The experimental knowledge of the polarization of neutrons elastically scattered from chromium is apparently confined to the 7.75 MeV studies of Dagge et al. [Dag+89]. Their results are shown in Fig. 5.1 together with the values calculated with the present CCM model. The agreement is acceptable, bearing in mind that no effort was made to adjust the CCM to describe polarization results. The present calculated results are very similar to those reported in ref. [Dag+89] using their "Cr1" potential. If a 4^+ state is added to the coupling scheme the agreement with experiment is somewhat improved [Dag+89]. If one considerably increases the spin-orbit strength, as suggested in ref. [Ols+90], the agreement with experimental polarization results deteriorates.

The spherical models (ISOM and ESOM) can not describe the obvious direct inelastic-neutron scattering processes, particularly those associated with the excitation of the 1.434 MeV state. However, they do give a reasonable description of inelastic scattering primarily due to compound-nucleus processes as observed in the earlier lower-energy work from this laboratory [GSW82], in the higher-energy excitations reported in ref. [KP74] and in the present work. The CCM model, inclusive of CN contributions, generally reproduces the differential cross sections for the excitation of the 1.434 MeV level up to ≈ 15 MeV, as illustrated in Fig. 4.6. Several of the experimental distributions indicated very-forward angle results considerably larger than the calculated values, e.g., the present work at 7.5 and 8.0 MeV. These larger values are not supported by the rest of the experimental data, and are probably the result of experimental distortions due to a "tail" on the much larger elastic-scattering peak. The general angular trends of the

Table 5.1. Measured and calculated strength functions in units of 10^{-4} .

Model	S_0	S_1
ESOM	2.93	0.527
ISOM	3.71	0.954
DSOM	3.67	0.613
CCM	3.28	0.938
Exp. [MDH81]	2.5 ± 0.9	0.52 ± 0.12

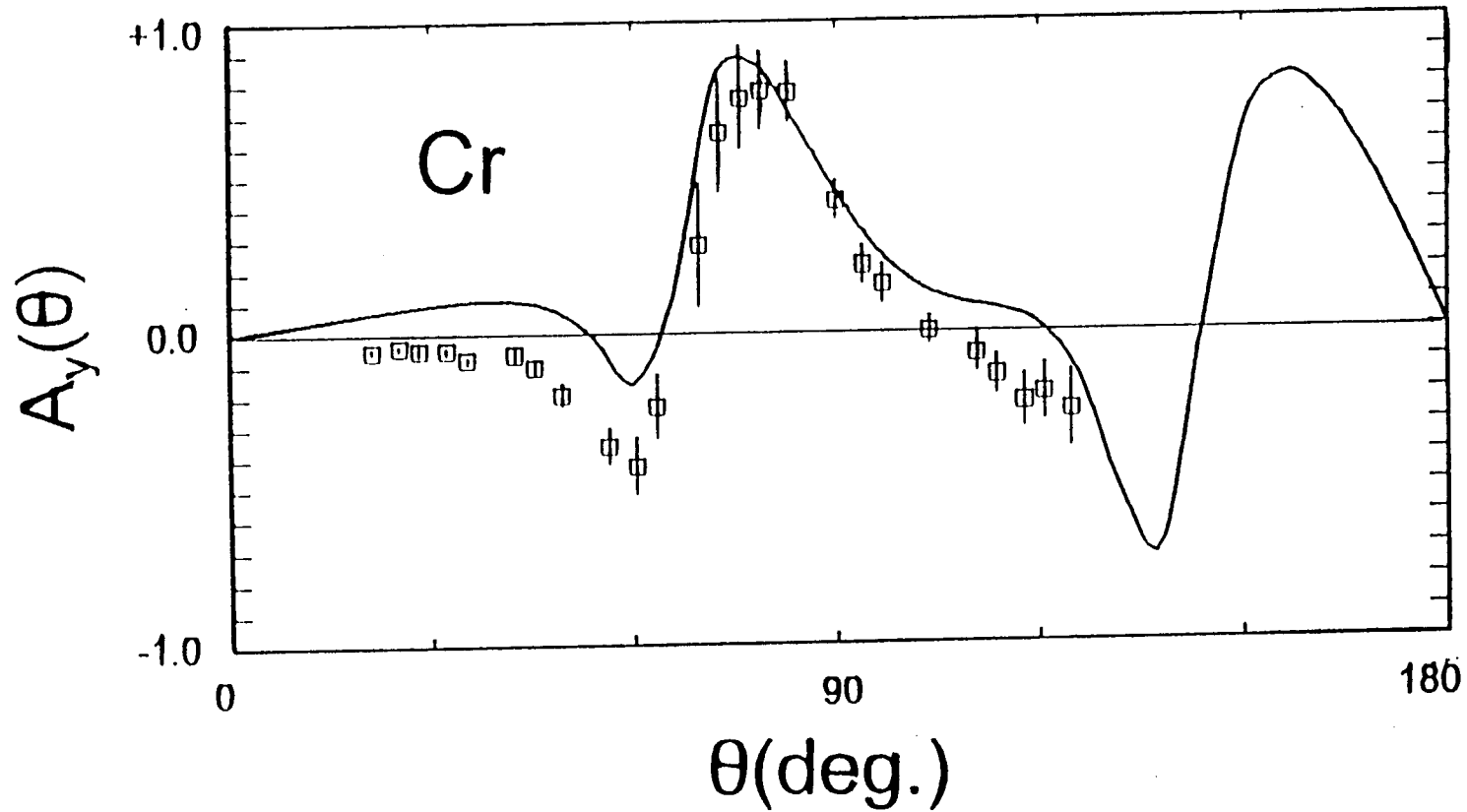


Fig. 5.1. Comparison of measured and calculated polarizations of 7.75 MeV neutrons elastically scattered from elemental chromium. The experimental values of ref. [Dag+89] are indicated by symbols and the curve was calculated with the CCM model.

calculations are qualitatively consistent with the measured values but there is a tendency to under predict the very back-angle scattering, particularly as the energy increases. The simplicity of the model used in the calculations may contribute to these differences as limited calculations using a two-phonon model somewhat alleviated the situation. There are large differences between measured and calculated inelastic differential distributions at 21.6 MeV, both in magnitude and in shape. The reason for this is not known, but it is noted that these particular experimental results are from the same measurements that gave the unusual elastic-scattering distributions cited above, and that the original authors experienced essentially the same problem in attempting to interpret their own measurements [Ols+90]. The CCM also gives a reasonable prediction of the angle-integrated cross sections for the excitation of the 1.434 MeV level up to at least 15 MeV, as illustrated by the lower curve in Fig. 3.4. There are some differences above 15 MeV but the experimental data is uncertain and discrepant. Near 5 MeV the results calculated with the statistical parameters of ref. [GC65] tend to be smaller than the present measured results. This region is sensitive to CN effects and thus to the exact choice of the statistical level parameters used in the model calculations. For example, increasing the "temperature" given in ref. [GC65] by 50% leads to the upper curve of Fig. 3.4 without significant changes in the other general model parameters. Such temperature changes are not unexpected as ^{52}Cr is magic in neutron number.

The present three potentials (ISOM, ESOM and CCM) are quite similar, with differences that in many ways may not be significant. The real strengths are very similar, falling from $\approx 490 \text{ MeV}\cdot\text{fm}^3$ at $E = 0$ with a slope of $\approx -5.0 \text{ fm}^3$, as illustrated for the CCM model in Fig. 5.2. This strength and slope are larger than frequently encountered in "global" spherical models (e.g., refs. [BG69], [RKF79], and [WG86]) or "global" studies of the real mean-field potential (e.g., ref. [Bau+82] which gives $J_v = 478.2 - 3.50 \cdot E + 0.0066 \cdot E^2 \text{ MeV}\cdot\text{fm}^3$ for neutrons incident on ^{52}Cr). The present real strengths are similar to those that have been reported from neutron scattering from nearby masses lying near the peak of the S_0 strength function (e.g., for neutron scattering from iron, refs. [AY81] and [Smi95]). The present chromium J_v values were compared with other chromium values deduced from both (n,n) and (p,p) measurements (see refs. [Per+70, Fab+80, Dag+89, Ols+87, Ols+90, Ste+65, Per+68, GSW82, Fun+64, Pre+70, Pas+70, HW71, And+64, Lom+72, Buc63, KD68 and Kos+67]). In making these comparisons the (p,p) results were corrected for coulomb effects using the conventional expression $V_c = 0.4 \cdot Z/A^{1/3}$, and converted to comparable (n,n) values assuming an isovector real-potential

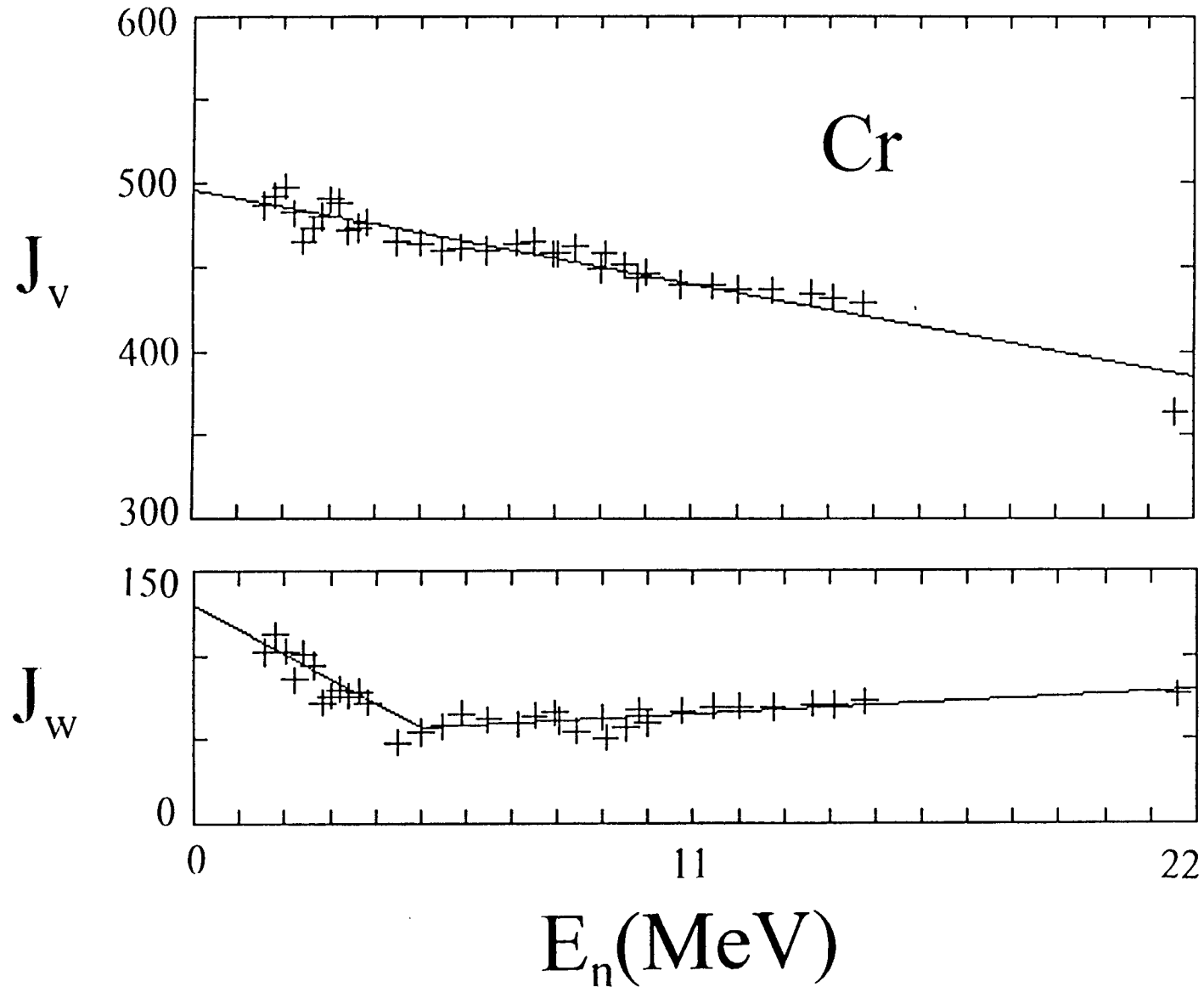


Fig. 5.2. Energy dependencies of the real- (J_v) and imaginary- (J_w) potential strengths of the CCM expressed as volume integrals per nucleon (in units of $\text{MeV}\cdot\text{fm}^3$). Symbols indicate the results obtained by individual fitting and curves the parameterization of Table 4.3.

depth (V_1) of 20 MeV. The latter correction is not particularly sensitive to the exact value of V_1 as the asymmetry is small. A linear fit to these published values above ≈ 10 MeV, where fluctuation and dispersion effects should be small, leads to an equivalent neutron real-potential strength of $J_v = 482.4 - 4.068 \cdot E \text{ MeV-fm}^3$, which is remarkably similar to the present results, particularly to the ESOM value. Generally, the large magnitude and energy dependence of $J_v(E \rightarrow 0)$ in the mass region of the maximum of the S_0 strength function is a recognized but unresolved physical issue. The real-potential diffusenesses of the three models are similar and have values that are "conventional". The a_v of the CCM and ESOM differ by only $\approx 2.7\%$ and are in good agreement with the ISOM value at the mid-point of the energy range. The slight energy dependence of the ISOM a_v is probably only an artifact of the fitting procedures, not reflecting isotopic perturbations. The three real-potential radii differ by $\approx 2.0 \rightarrow 2.5\%$ over the relevant energy range. That is remarkable agreement given the strong correlation between real-potential depth and radius (i.e., the Vr^2 anomaly). r_v values found in the literature scatter widely, and in some cases they have simply been assumed in the interpretations (typically choosing $r_v = 1.25 \text{ fm}$). However, there is a trend for the previously reported lower-energy (p,p) and (n,n) r_v values to be larger than at higher energies. That is consistent with the energy dependencies of the present r_v values, which are to be expected due to the dispersion relationship discussed below. The imaginary-potential strengths of the three potentials are qualitatively similar. As illustrated in Fig. 5.2 for the CCM, they all slowly increase with energy above ≈ 5 to 6 MeV. The rate of increase is largest and the magnitude the smallest for the CCM, as is expected, as more channels are explicitly accounted for in the CCM calculations. At lower energies (below $\approx 5 \rightarrow 6$ MeV) all three imaginary-potential strengths rapidly increase with decreasing energy to quite large values at $E \approx 0$. Such unusual behavior has been observed in this mass region of large S_0 strength functions ([Smi95], [Ped+88]), and represents a change of the character of the potential as the energy decreases below ≈ 5 MeV. A consequence is smaller total cross sections at low energies, more consistent with the energy averages of the experimental values. The three imaginary-potential radii are of qualitatively the same size and all decrease with energy to quite small values at ≈ 20 MeV. The energy dependence is sharper than for similar iron studies [Smi95] and may suggest some shortcomings in the underlying model assumptions. The imaginary-potential diffusenesses are also qualitatively similar, and all of them decrease with decreasing energy to quite small values as $E \rightarrow 0$ in a manner that has been widely observed at this

laboratory. All of the present potentials are devoid of volume absorption. It is introduced in various global models at ≈ 12 MeV (e.g., ref. [RKF79]) and increases with energy to relatively small values at ≈ 25 MeV. Fitting of the present elastic-scattering data with the inclusion of a volume absorption component led to no improvement in the description of the data. However, that conclusion depends very largely on the single 21.6 MeV elastic distribution. The authors of that particular data set also concluded that volume absorption was not a factor in the SOM interpretation of their data [Ols+87]. Of course, all of the interpretations of the present work are rigorously applicable only to incident-neutron energies of $\lesssim 22$ MeV. In particular, some of the parameter energy dependencies can not continue indefinitely, and the relevant parameters must asymptotically approach some constant values as energies increase above ≈ 22 MeV. However, it is remarkable that at least some aspects of the present potentials are supported by (p,p) studies to ≈ 40 MeV, (e.g., the strength and energy dependence of J_v).

The extensive CCM fitting procedures were repeated for values of β_2 $0.1 \rightarrow 0.275$ in steps of 0.025. Reasonable descriptions of the elastic scattering were obtained for each β_2 value, providing no clear guidance as to the selection of β_2 . However, fitting the inelastic cross sections for the excitation of the 1.434 MeV 2^+ level clearly indicated that $\beta_2 = 0.20 \pm \approx 0.01$. Approximately 84% of elemental chromium consists of ^{52}Cr ($N = 28$). Thus it is expected that the deformations should be reasonably consistent with the predictions of the core-coupling model of Madsen, Brown and Anderson [MBA75, BM75] which predicts collective proton vibrations with a β_2 for the neutron interaction larger than for the proton interaction, and smaller or approximately the same as for the electro-magnetic interaction. The interaction strengths are geometry dependent and thus comparisons should be made in terms of the deformation length, $\delta = \beta_2 \cdot R$, where R is usually taken to be the real-potential radius [Bla63]. R_v is slightly energy dependent in the present CCM model. There are a few (n,n) measurements and interpretations reported in the literature that give the β_2 of ^{52}Cr at a variety of energies. At 7.75 MeV the reported $\delta_{nn} = 0.926$ fm, or 2.5% smaller than given by the CCM [Dag+89]. At 14 MeV the reported value is $\delta_{nn} = 0.979$ fm, or 4.2% larger than given by the CCM [Ste+65]. At 21.6 MeV the reported $\delta_{nn} = 0.974$ fm, or 5.1% larger than given by the CCM [Ols+90]. These interpretations used both coupled-channels and DWBA methods. The agreement with the present δ_{nn} results is remarkably good (i.e., to within $\leq 5\%$, or the estimated

uncertainty in the present measurements. The same comparisons can be made with the results of (p,p) measurements and interpretations. δ_{pp} values are 0.815 fm at 11 MeV [Per+70], 0.779 fm at 35 MeV [Fab+80] and 0.77 fm at 40 MeV [Pre+70]. All of these values are 13.5 → 14.0% smaller than the predictions of the present CCM (furthermore, ref. [Fun+64] concludes that $\delta_{em}/\delta_{pp} \approx 1.15$ at ≈ 17.5 MeV). It is remarkable that the difference is so constant given the very large energy range of the comparisons. The comparative $\delta_{em} = 1.003$ fm follows from the compilation of Raman et al [Ram+87] based upon coulomb-excitation studies. This value can be compared with the $\delta_{nn}(E \rightarrow 0) = 0.964$ fm of the present CCM. Thus the present CCM and results available in the literature indicate that δ_{pp} is less than δ_{nn} by approximately 13.5 → 14.0%, while δ_{nn} is approximately the same as δ_{em} , or possibly a little smaller. These conclusions are remarkably consistent with the core-coupling model.

The present CCM uses a very simple one-phonon representation of what doubtless is a far more complex situation. The next step in complexity may be the inclusion of higher-order phonons. That alternative was examined with a one- and two-phonon model using identical fitting procedures to those described above at selected energies. There was no noticeable improvement in the quality of the model results. In particular, the calculated elastic distributions were in no better agreement with the measured values than the results of the simple one-phonon model, and the inelastic-scattering cross sections for the excitation of the 1.434 MeV 2^+ level did not change by appreciable amounts in either magnitude or angular shape. The same conclusions were reached with an anharmonic vibrator and with the addition of a 3^- level at 4.56 MeV to the coupling scheme with various β_3 values. Underlying all of the present CCM interpretations is the assumption that ^{52}Cr behaves as a vibrator. This assumption is supported by the results of a number of charged-particle studies (e.g., see ref. [Bay+69]), and by considerations of the low-energy excited structure of ^{52}Cr (e.g., see ref. [Fun+64]). An extreme alternative to the CCM vibrational model is a simple rotational model. The fitting was repeated with that assumption and a $\beta_2 = 0.20$ with results that were essentially the same as obtained with the one-phonon vibrational model. Thus the neutron reactions do not clearly delineate the qualitative character of the collective behavior of ^{52}Cr .

The present neutron-scattering studies do not directly establish the asymmetry ($\eta \equiv (N-Z)/A$) dependence of the potential. However, comparisons with proton potentials found in the literature give an indication of the asymmetry effect. The

compilation of Perey and Perey [PP76] cites fourteen spherical proton optical potentials relevant to the incident energy range $\approx 10 \rightarrow 20$ MeV. Three of these appear anomalous and were abandoned. The real-potential strengths of the remaining eleven, expressed as volume-integrals-per-nucleon (J), are relatively consistent. When corrected for coulomb effects, they are comparable with the present neutron SOM through the well-known expression [Lan62] $J = J_0 (1 \pm \xi \cdot \eta)$, where ξ is a constant and \pm (-) pertains to proton (neutron) potentials. All the proton real-potential strengths are larger than the respective values from the present SOM. The energy dependence of the proton potentials is $\approx 15\%$ smaller than that of the SOM. This is reasonable agreement considering the limited scope and scatter of the proton potentials, and tends to support the relatively strong energy dependence of the SOM real potential. Comparisons of neutron and proton real-potential strengths in the energy range $\approx 10 \rightarrow 20$ MeV lead to values of ξ varying from ≈ 0.5 to 0.7 , increasing with incident energy. This range of results is qualitatively consistent with $\xi = 0.48$ suggested by the theory of nucleon-nucleon scattering [TT67, GPT68]. Thus, what is known of chromium proton potentials tends to support the real potential of the present models. Similar comparisons are applicable to imaginary potentials but the scatter of the proton results is too large for meaningful interpretations. Of course, proton potentials can offer no guidance to the behavior of the neutron potential at low energies well below the coulomb barrier where the present interpretations suggest rapidly changing imaginary strengths.

It is well known that dispersion effects distort model interpretations, such as described above, particularly the energy dependence of some of the model parameters. The dispersion relationship results in a real-potential strength given by

$$J_V(E) = J_{HF}(E) + \frac{P}{\pi} \int_{-\infty}^{+\infty} \frac{J_{WS}(E')}{E - E'} dE', \quad (1)$$

where J_{HF} is the strength of the local-equivalent Hartree-Fock potential, J_{WS} is the strength of the surface-imaginary potential, and P denotes the principle value of the integral [Sat83]. The qualitative effect of the integral of Eq. 1 is to add a surface component to the real SW potential used in the above models. Quantitative assessment of the contribution is difficult in the present case as the contribution is most significant at low energies where the experimental data fluctuates by appreciable amounts. However, in the present work the contribution of the dispersion integral was estimated using the methods of refs. [Smi94] and [Smi95]. The approach was an iterative procedure starting with the above ISOM potential. In doing so the anomalous low-energy behavior of the ISOM J_w was

ignored. The surface J_w was assumed to be the high-energy branch of Table 4.2 from zero to 25 MeV, and then to fall in a linear manner to zero at 60 MeV. Concurrently, it was assumed that a volume J_w commenced at 25 MeV and increased in a linear manner to $95 \text{ MeV}\cdot\text{fm}^3$ at 60 MeV and then remained constant. From $E = 0$ to the fermi energy (E_F) J_w was given a quadratic energy dependence. J_w was assumed to be symmetric about E_F which was taken to be -9.99 MeV as calculated from the mass tables [JLM77]. With these reasonable assumptions, the surface addition to J_{HF} at $E = 0$ was $\approx 0.7 \cdot J_w$, and decreased with energy in a monotonic manner to negligible values at 25 MeV. The entire ISOM fitting procedure was repeated including the dispersion contribution and resulted in the model parameters given in Table 5.2 (herein referred to as the "DSOM"), and the description of the differential elastic scattering shown in Fig. 5.3. The quality of the fits to the data is essentially the same as that obtained with the simple ISOM and (see Fig. 4.4). ISOM and DSOM total cross section results were also very similar, as were the strength functions (see Table 5.1). Comparing Tables 4.2 and 5.2, there are some obvious differences between ISOM and DSOM potentials. These are primarily in the real potential where the J_v of the ISOM is considerably the larger at lower energies, as it should be since it includes the contribution of the integral of Eq. 1, while J_v for the DSOM should be the J_{HF} alone. The difference is consistent with calculated value of the integral of Eq. 1. It is clear that the slope of J_v in a simple SOM interpretation will be biased by the dispersion integral which in turn will vary depending upon the fermi energy, and the magnitude of the $^{52}\text{Cr } E_F$ is quite large. The DSOM r_v is energy independent, in contrast to that of the ISOM. This difference is consistent with the energy dependent surface component of the real potential predicted by the dispersion integral. The ISOM and DSOM imaginary potentials are quite similar except at the lowest energies where the reliability of the fitting is compromised by fluctuations. The inclusion of the dispersive effects does not significantly improve the phenomenological description of the neutron data but it does alter some of the underlying physical concepts (e.g., J_v is essentially J_{HF} for the DSOM and considerably larger for the ISOM). Such differences are very often ignored in physical discussions. The dispersion effects are more sensitive in the bound region due to the contribution of the integral of Eq. 1. There is a large body of information on nucleon-transfer and knock-out reactions in the literature from which neutron particle- and hole-state binding energies can be determined. A summary of much of this information and a systematic representation is given by Millener and Hodgson

Table 5.2. Potential parameters of the dispersive DSOM of the text. The nomenclature is identical to that of Fig. 4.1.

Real Potential

$$\begin{aligned}J_v &= 428.5 - 1.4092 \cdot E \\r_v &= 1.2268 \\a_v &= 0.5355 + 0.0059257 \cdot E\end{aligned}$$

Imaginary Potential

$$\begin{aligned}J_w &= 118.0 - 7.784 \cdot E \quad (E < 6) \\&= 65.3 + 1.1503 \cdot E \quad (E \geq 6) \\r_w &= 1.2955 - 0.012523 \cdot E \\a_w &= 0.13 + 0.083154 \cdot E \quad (E < 6) \\&= 0.6428 + 0.0023867 \cdot E \quad (E \geq 6)\end{aligned}$$

Spin-orbit Potential

$$\begin{aligned}V_{so} &= 5.921 - 0.015 \cdot E \\r_{so} &= 1.103 \\a_{so} &= 0.560\end{aligned}$$

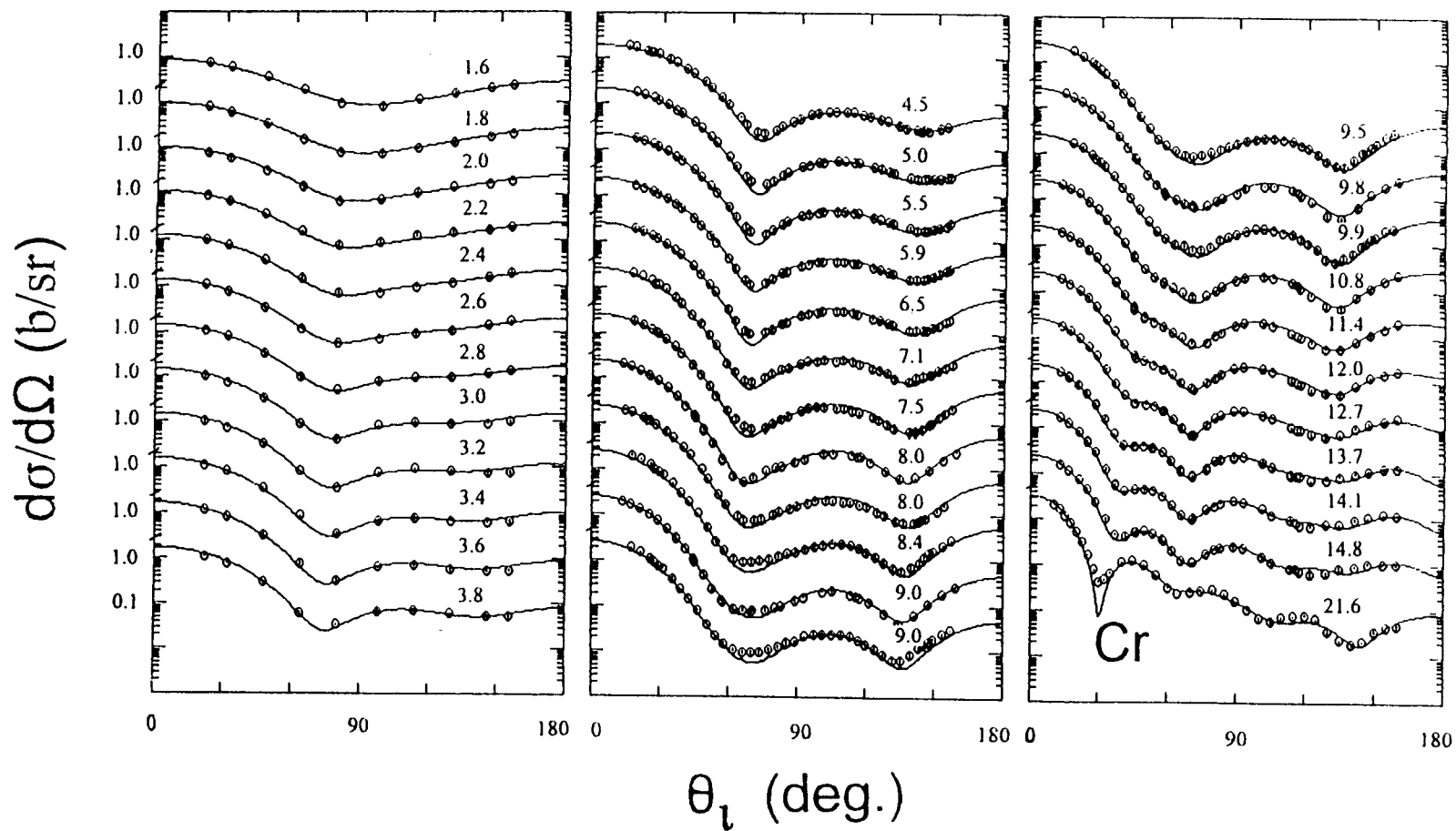


Fig. 5.3. Comparison of the measured elastic-scattering data base (symbols) with the results of DSOM calculations (curves). Approximate incident-neutron energies are numerically noted in MeV.

[MH73]. Following those authors and ref. [Bay66], neutron particle- and hole-state binding energies were calculated with the DSOM, ISOM and ESOM potentials and are compared with the relevant experimental results in Table 5.3. The DSOM results arguably give a slightly better overall agreement with the experimental results, but there are not marked differences in the quality of the description of the experimental results. This is not surprising as a number of uncertainties are involved in such binding-energy calculations. The calculated values given in Table 5.3 explicitly used the cited potentials, including the energy dependencies of geometric parameters. It is not at all clear that these energy dependencies, based upon neutron interpretations at modest unbound energies (< 22 MeV), should be extrapolated deep into the bound region. However, repeating the calculations with the geometries fixed at the $E = 0$ values did not greatly change the results. The calculations of Table 5.3 assumed an isovector potential strength of 32 MeV, following the work of ref. [MH73]. A more reasonable value of 24 MeV did not greatly change the results. Throughout it was assumed that the isoscalar and isovector potentials have the same geometric shape which is not necessarily true. All of the comparisons are based upon the assumption that ^{52}Cr is a spherical nucleus which is not necessarily true. However, the first-order effect of introducing a deformation should not be large (see ref. [MH73A]).

Acknowledgments

The authors are indebted to Dr. J. Raynal for the provision of the coupled-channels computational programs ECIS94 and ECIS95 and of extensive instructions on their use, and to Dr. P. E. Hodgson for charged-particle-reaction suggestions.

Table 5.3. Comparison of measured and calculated neutron particle and hole binding energies (in MeV)

State ^a	Exp. ^b	DSOM	ISOM	ESOM
$2s_{1/2}$				
Hole, $T_{<}$	14.93	17.02	20.32	19.65
Hole, $T_{>}$	21.00	23.80	26.57	25.71
$2p_{1/2}$				
Part., $T_{>}$	5.22	7.33	6.66	5.89
$2p_{3/2}$				
Part., $T_{>}$	7.00	8.50	8.45	7.67
$1d_{3/2}$				
Hole, $T_{<}$	14.93	17.47	20.53	19.34
Hole, $T_{>}$	20.61	24.38	26.82	25.49
$1f_{5/2}$				
Part., $T_{>}$	4.55	8.29	7.34	5.50
$1f_{7/2}$				
Part., $T_{>}$	10.26	12.76	15.29	13.01
$1f_{7/2}$				
Hole, $T_{<}$	12.74	12.15	16.42	13.99
Hole, $T_{>}$	18.93	16.05	23.14	19.99

^a Nomenclature of ref. [MH73].

^b Values taken from the experimental compilation and systematics of ref. [MH73].

References

- [And+64] P. T. Andrews, R. W. Clifft, L. L. Green and Sharpey-Schafer, Nucl. Phys. 56 449 (1964).
- [AY81] E. Arthur and P. G. Young, Los Alamos National Laboratory Report, LA-8626-MS (1981).
- [Bau+82] M. Bauer, E. Hernandez-Saldana, P. E. Hodgson and J. Quintanilla, J. Phys. G8 525 (1982).
- [Bay66] B. F. Bayman, Isobaric spin in nuclear physics p. 503 (Academic, New York, 1966).
- [Bay+69] B. F. Bayman, D. R. Bes and R. A. Broglia, Phys. Rev. Lett. 23 1299 (1969).
- [BG69] F. G. Becchetti and G. W. Greenlees, Phys. Rev. 182 1190 (1969).
- [Bla63] J. S. Blair, Direct interactions and nuclear reaction mechanisms p. 666 (Gordon and Breach, New York, 1963).
- [BM75] V. R. Brown and V. A. Madsen, Phys. Rev. C11 1298 (1975).
- [Buc63] B. Buck, Phys. Rev. 130 712 (1963).
- [Cie+68] S. Cierjacks, P. Forti, D. Kopsch, L. Kropp, J. Nebe and H. Unseld, Institute fur Angewandte Kernphysik Report, KFK-1000 (1968).
- [CL55] L. Cranberg and J. Levin, Proc. Conf. on Peaceful Uses of Atomic Energy, (United Nations Press, New York, 1955).
- [CL56] L. Cranberg and J. Levin, Phys. Rev. 103 343 (1956).
- [CSL83] Nuclear Standards File, IAEA Tech. Report 227, eds. H. Conde, A. Smith and A. Lorenz (IAEA Press, Vienna, 1983).
- [Dag+89] C. Dagge, W. Grum, J. W. Hammer, K. W. Hoffmann and G. Schreder, Phys. Rev. C39 1768 (1989).
- [Dro87] M. Drosig, IAEA Report, IAEA-TECDOC-410 (IAEA Press, Vienna, 1987).
- [Fab+80] E. Fabrici, S. Micheletti, M. Pignanelli, F. G. Resmini, R. De Leo, D. D'Erasmus and A. Pantaleo, Phys. Rev. C21 844 (1980).
- [Fun+64] H. O. Funsten, N. R. Roberson and E. Rost, Phys. Rev. B134 117 (1964).
- [GC65] A. Gilbert and A. Cameron, Can. J. Phys. 87 362 (1965)
- [GPT68] G. W. Greenlees, G. J. Pyle and Y. C. Tang, Phys. Rev. 171 1115 (1968).
- [GSW82] P. T. Guenther, A. B. Smith and J. F. Whalen, Nucl. Sci. and Eng. 82 408 (1982).
- [Hod71] P. E. Hodgson, Nuclear reactions and nuclear structure (Clarendon, Oxford, 1971).
- [Hom+69] B. Holmqvist et al., Studsvik Report, AE-366 (1969).
- [HF52] W. Hauser and H. Feshbach, Phys. Rev. 87 362 (1952).
- [HW71] B. Holmqvist and T. Wiedling, Studsvik Report, AE-430 (1971).
- [JLM77] J. P. Jeukenne, A. Lejeune and C. Mahaux, Phys. Rev. C16 80 (1977); also Phys. Rev. C15 10 (1977).
- [Joh+85] I. P. Johnson, D. Halderson, J. A. Carr and F. Petrovich, Phys. Rev. C32 103 (1985).

- [KD68] P. Kossanyi and R. deSwiniarski, Nucl. Phys. A108 577 (1968).
- [Kos+67] P. Kossanyi-Demay, R. deSwiniarski and C. Glashausser, Nucl. Phys. A94 513 (1967)
- [KP74] W. E. Kinney and F. G. Perey, Oak Ridge National Laboratory Report, ORNL-4806 (1974).
- [Lan62] A. M. Lane, Nucl. Phys. 35 676 (1962).
- [LHH81] D. Larsen, J. Harvey and N. Hill, Oak Ridge National Laboratory Report, ORNL-5787 (1981).
- [Lom+72] J. C. Lombardi, R. N. Boyd, R. Arking and A. B. Robbins, Nucl. Phys. A192 641 (1972).
- [MBA75] V. A. Madsen, V. R. Brown and J. D. Anderson, Phys. Rev. C12 1205 (1975).
- [MBZ64] J. D. McCullen, B. F. Bayman and L. Zamick, Phys. Rev. 134 B637 (1964).
- [MDH81] S. Mughabghab, M. Divadeenam and N. Holden, Neutron cross sections (Academic, New York, 1981).
- [MH73] D. J. Millener and P. E. Hodgson, Nucl. Phys. A209 59 (1973).
- [MH73A] F. Malaguti and P. E. Hodgson, Nucl. Phys. A215 243 (1973).
- [Mol80] P. A. Moldauer, Nucl. Phys. A344 185 (1980).
- [Mol81] P. A. Moldauer, Spherical optical-model code ABAREX, private communication (1982), modified for elemental use by S. Chiba.
- [Mol82] P. A. Moldauer, Coupled channels code ANLECIS, private communication (1982); a version of ECIS79 [Ray94].
- [MW66] J. Meadows and J. Whalen, Argonne National Laboratory Report, ANL-7210 (1966).
- [NDS] T. W. Burrows, Nucl. Data Sheets 42 369 (1984); Huo Junde, Hu Dailing, Nucl. Data Sheets 43 481 (1984); Huo Junde, Hu Dailing, Sun Huibin, You Janming and Hu Baohua, Nucl. Data Sheets 56 677 (1989); Wang Gongqing, Zhu Jiabi and Zhang Jingen, Nucl. Data Sheets 50 255 (1987).
- [NNDC] National Nuclear Data Center, Brookhaven National Laboratory, Upton, New York.
- [Ols+87] N. Olsson, B. Trostelle, E. Ramstroem and B. Holmqvist, Nucl. Phys. A472 237 (1987).
- [Ols+90] N. Olsson B. Trostell and E. Ramstroem, Nucl. Phys. A513 205 (1990).
- [Pas+70] M. V. Pasechnik et al., Sov. J. Nucl. Phys. 11 533 (1970).
- [Ped+88] R. S. Pedroni, C. R. Howell, G. M. Honore, H. G. Pfutzer, R. C. Byrd, R. L. Walter and J. P. Delaroche, Phys. Rev. C38 2052 (1988).
- [Per+68] C. M. Perey, F. G. Perey, J. K. Dickens and R. J. Silva, Phys. Rev. 175 1460 (1968).
- [Per+70] C. M. Perey, R. J. Silva, J. K. Dickens and F. G. Perey, Phys. Rev. C2 468 (1970).
- [PP76] C. M. Perey and F. G. Perey, At. Data and Nucl. Data Tables 17 1 (1976)
- [Pre+70] B. M. Preedom, C. R. Gruhn, T. Y. T. Kuo and C. J. Maggiori, Phys. Rev. C2 166 (1970).

- [Ram75] E. Almen-Ramstroem, Studsvik Report, AE-503 (1975).
- [Ram+87] S. Raman, C. H. Marlarkey, W. T. Miller, C. W. Nester Jr. and P. H. Stelson, At. Data and Nucl. Data Tables, 36 1 (1987).
- [RKF79] J. Rapaport, V. Kulkarni and R. W. Finlay, Nucl. Phys. A330 15 (1979).
- [Ray94] J. Raynal, Coupled-channels computer codes ECIS79, ECIS94 and ECIS95, NEA memorandum, unpublished (1979); also CEA Report, CEA-N-2772 (1994).
- [Sat83] G. R. Satchler, Direct nuclear reactions (Clarendon, Oxford, 1983).
- [Sch+94] D. Schmidt, W. Mannhart, H. Klein and R. Nolte, Physikalisch-Technische Bundesanstalt Braunschweig Report, PTB-N-20 (1994).
- [SM96] D. Schmidt and W. Mannhart, private communication (1996), to be published.
- [Smi91] A. B. Smith, Argonne National Laboratory memorandum, unpublished (1991).
- [Smi94] A. B. Smith, Nucl. Phys. A576 165 (1994).
- [Smi95] A. B. Smith, Neutron scattering and models:- iron, accepted for publication in Nucl. Phys.
- [Smi+92] A. B. Smith and P. T. Guenther, Argonne National Laboratory Report, ANL/NDM-127 (1992); S. Chiba, P. Guenther, A. Smith, M. Sugimoto and R. Lawson, Phys. Rev. C45 1260 (1992); C. Budtz-Jorgensen, P. Guenther, A. Smith and J. Whalen, Z. Phys. A306 2656 (1982); A. Smith, P. Guenther, R. Larsen, C. Nelson, P. Walker and J. Whalen, Nucl. Instru. and Methods, 50 277 (1967); and references cited therein.
- [Ste+65] P. H. Stelson, R. L. Robinson, H. J. Kim, J. Rapaport and G. R. Satchler, Nucl. Phys. 68 97 (1965).
- [TO67] J. H. Towle and R. O. Owens, Nucl. Phys. A100 257 (1967)
- [TT67] D. R. Thompson and Y. C. Tang, Phys. Rev. 159 806 (1967).
- [WG86] R. L. Walter and P. P. Guss, Proc. Conf on Nucl. Data for Basic and Applied Sci., eds. P. Young et al., v. 2, p. 277 (Gordon and Breach, New York, 1986).
- [Yam+90] Y. Yamanouti, M. Sugimoto, M. Mizumoto, Y. Watanabe and K. Hasegawa, NEA Report, NEANDC(J)-155 (1990).